Gradient structures for the thermomechanics of shape-memory materials

Ferdinando Auricchio [a,c], Elisa Boatti [a,*], Alessandro Reali [a,c,d], Ulisse Stefanelli [a,b,c]

[a] *Department of Civil Engineering and Architecture, University of Pavia, via Ferrata 3, 27100 Pavia, Italy*
[b] *Faculty of Mathematics, University of Vienna, Oskar-Morgenstern-Platz 1, 1090 Vienna, Austria*
[c] *Istituto di Matematica Applicata e Tecnologie Informatiche E. Magenes - CNR, v. Ferrata 1, 27100 Pavia, Italy*
[d] *Institute for Advanced Study, Technische Universität München, Lichtenbergstraße 2a, 85748 Garching, Germany*

Abstract

We investigate the variational structure of a phenomenological model for the coupled thermomechanical behavior of shape-memory polycrystalline materials. The nonisothermal evolution of the medium is reformulated as a generalized gradient flow of the entropy with respect to an entropy-production potential. Based on this reformulation, a semi-implicit time-discretization of the fully coupled thermomechanical problem is presented and proved to be unconditionally stable and convergent. The flexibility and robustness of the numerical method is assessed via both uniaxial and multiaxial computational tests.
ⓒ 2015 Elsevier B.V. All rights reserved.

1. Introduction

Shape-memory alloys (SMA) are *active* materials: considerably large deformations (up to 10%) can be activated either by mechanical or thermal means. Such amazing material properties, combined with the typical resistance and workability of metals, make SMAs attractive for innovative engineering applications in various industrial fields including, e.g., automotive, robotics, civil, seismic, and biomedical [1]. The interest for this class of materials is currently triggering intense research efforts toward the implementation of appropriate constitutive models capable of efficiently and robustly reproduce the SMA behavior. The SMA response is a genuinely coupled thermomechanical effect. As such, the accurate and efficient treatment of nonisothermal situations bears a crucial importance.

The present paper investigates the variational structure of the three-dimensional thermo-mechanical constitutive model, firstly presented in [2], and then reformulated in [3] and [4]. Our interest in this model is motivated by

---

its capability of qualitatively reproducing the macroscopic behavior of SMAs within a simple (in terms of number of material parameters) variational frame: in the isothermal situation the evolution of the medium is driven by the interplay of energy storage and dissipation mechanism within the frame of Generalized Standard Materials [5–7]. A second crucial advantage of this model in comparison with others is its amenability to a complete mathematical and numerical discussion. The nonlinear constitutive material relations and the corresponding quasistatic evolution systems can be rigorously proved to admit solutions, which are limits of stable space–time discretizations, see the recent survey [8]. Moreover, the experimental validation of the model by comparison with test data on NiTi wires and springs is also available in [9,10].

The aim of the this paper is to investigate further the structure of the model [2,3] by presenting a new variational formulation of the full nonisothermal model. This consists in a *generalized gradient flow* of the *total entropy* $y \mapsto \mathcal{S}(y)$ as a function of the state vector y, including temperature as well as mechanical and internal variables. In particular, we shall be considering the following differential system

$$\partial_{\dot{y}} \mathcal{K}(t, y; \dot{y}) - \partial \mathcal{S}(y) \ni \mathbf{0}, \tag{1.1}$$

where $\mathcal{K}(t, y; \cdot)$ corresponds to the *entropy-production potential*. Here, the dot represents differentiation with respect to time whereas ∂ stands for some suitable notion of gradient, to be detailed below. The symbol $\ni$ refers to the fact that, in absence of smoothness, the left hand side terms in (1.1) can be sets. As $\mathcal{K}$ depends not only on the rate $\dot{y}$ but also on the state y, we refer to (1.1) as a *generalized* gradient flow.

The variational formulation (1.1) for nonisothermal evolution is unprecedented in the frame of the model in [2,3]. The interest in such perspective relies on the possibility of exploiting this variational structure both for the theoretical and the numerical discussion of the model. Different choices for $\mathcal{K}$ will be presented, all satisfying the following fundamental structural property

for all (t, y) the map $\dot{y} \mapsto \mathcal{K}(t, y; \dot{y})$

is convex, nonnegative, and $\mathcal{K}(t, y; \mathbf{0}) = 0$. $\tag{1.2}$

This structural property immediately entails the *dissipativity* of the evolution. By assuming sufficient smoothness, one can multiply both sides of (1.1) by $\dot{y}$ and obtain

$$\frac{\mathrm{d}}{\mathrm{d}t} \mathcal{S}(y) = \partial \mathcal{S}(y) \cdot \dot{y} = \partial_{\dot{y}} \mathcal{K}(t, y; \dot{y}) \cdot \dot{y} \geq \mathcal{K}(t, y; \dot{y}) \geq 0$$

where we have used the convexity of $\dot{y} \mapsto \mathcal{K}(t, y; \dot{y})$ as well as the fact that $\mathcal{K}(t, y; \mathbf{0}) = 0 = \min \mathcal{K}(t, y; \cdot)$. In particular, the entropy increases along all sufficiently smooth evolutions.

The phrasing of the full thermomechanical problem as (1.1) is inspired to the theory of General Equations for Non-Equilibrium Reversible–Irreversible Coupling (GENERIC). Introduced by Grmela & Öttinger [11,12] and recently reinterpreted by Mielke in a series of contributions [13,14], GENERIC provides a far-reaching variational paradigm for reformulating in a thermodynamically consistent way a variety of physical systems. In particular, GENERIC is tailored to the unified treatment of reversible and irreversible (or even hysteretic) dynamics. GENERIC has recently attracted increasing attention and has been applied to a number of situations ranging from complex fluids, to dissipative quantum mechanics [14], to thermomechanics [13], and to the Vlasov–Fokker–Planck equation [15].

The novelty of this paper is twofold. At the modeling level, we present a new variational formulation of the thermomechanically coupled system. As already commented, this formulation directly entails the dissipativity of the flow. In addition, we are able to include external actions in the picture. Let us mention that, up to now, the GENERIC framework is restricted to the description of *isolated* systems [16]. At first, we systematically eliminate the mechanical part from the problem by solving the quasistatic equilibrium system. This procedure allows us to consider body and traction forces, see Section 3.1. Then, by specifically reducing to the space-homogeneous case, we allow equilibration with a given external temperature, see Section 3.4.

A second novelty of the paper consists in presenting an unconditionally stable and convergent time-discrete scheme for the fully coupled thermomechanical system. Up to now the only available results in the nonisothermal case were restricted to the case of a given temperature [17,18], to viscous materials [19], or to one space dimension [20,21]. By making use of the new variational formulation (1.1) we are here able to tackle the three-dimensional case without assuming viscosity, although for space-homogeneous temperatures. By discretizing the system at the level of driving functionals, we directly obtain a numerical scheme reproducing the basic properties and, in particular, the dissipativity

the model. As a by-product of the convergence proof, we also establish the existence of a strong solution to the system in the continuous-time setting.

The prediction of the coupled thermomechanical response in polycrystalline SMA materials has attracted a remarkable attention in the last decades and the corresponding literature is extensive. By restricting to the case of macroscopic thermomechanically coupled systems, which are the most relevant for our purposes, we shall however minimally mention the models in [22–31]. A comprehensive review is to be found in [27,32]. In comparison with other available phenomenological models capable of reproducing thermomechanical couplings, see for instance the recent [33–36], our modeling choice has the distinctive advantage of allowing a rigorous mathematical discussion: numerical evidence is here supported by a complete theory. In addition, the variational formulation (1.1) paves the possibility of extending the reach of the present analysis to the various extensions of the model [2,3] which have been progressively proposed in order to deal with asymmetric behavior [37], magnetic effects [38–41], residual plasticity [42,43], and finite strains [44,44,45]. A complete space–time scheme based on (1.1) along the lines of [46] is the subject of a forthcoming paper.

We shall refer to Peigney & Seguin [47,48] for an alternative analysis towards a variational formulation of nonisothermal evolution problems in Generalized Standard Materials. In particular, in [47,48] the authors focus on the time incremental step and augment the time-discrete relations by means of additional terms in order to let the corresponding nonlinear system be symmetric, hence the gradient of some potential energy. These additional terms turn out to be consistent in case of continuous temperature evolution. The incremental step is then solved by minimization. Our approach is completely different as we propose a variational frame making sense at both the continuous and the discrete level simultaneously.

The paper is organized as follows: in Section 2 we present a detailed account of the model and prove its dissipative character. The generalized-gradient-flow reformulation of the thermomechanical problem is presented in Section 3. In particular, we specifically treat the general nonisothermal case as well as the case of space-homogeneous fields. A semi-implicit, variationally informed time-discrete scheme for the thermo-mechanical space-homogeneous problem is studied in Section 4. In particular, its unconditional stability and convergence are established. The corresponding numerical implementation is reported in Section 5 together with a number of computational results assessing the performance of the model. Eventually, conclusions are summarized in Section 6.

2. Model

The aim of this section is to recall the basic features and the notation of the thermomechanical model. This has been introduced in the isothermal case in [2] and then combined with finite elements in [3,4,49] and analyzed in [50]. The case of a given, nonconstant temperature has been discussed in [17,18] whereas the full thermomechanical coupling is investigated in [20,21] in one space dimension. The reader is referred to the recent survey [8] for details on the extension of the model to finite strains [44,45,51], residual plasticization [42,43,52,53], asymmetric behaviors [37], magnetic effects [19,38–40,54], as well as for space discretization [46,55] and control [41,56,57].

2.1. Tensors

In the following, bold Latin letters stand for both vectors and 2-tensors, and double-capital letters are for 4-tensors, all of which in $\mathbb{R}^3$. Given the 2-tensors $\boldsymbol{\alpha}$, $\boldsymbol{\beta} \in \mathbb{R}^{3 \times 3}$ and the 4-tensor $\mathbb{A} \in \mathbb{R}^{3 \times 3 \times 3 \times 3}$ we classically define $\boldsymbol{\alpha} : \boldsymbol{\beta} \in \mathbb{R}$ and $\mathbb{A}\boldsymbol{\beta} \in \mathbb{R}^{3 \times 3}$ as (summation convention) $\boldsymbol{\alpha} : \boldsymbol{\beta} := \alpha_{ij}\beta_{ij}$ and $(\mathbb{A}\boldsymbol{\beta})_{ij} := A_{ij\ell k}\beta_{\ell k}$, respectively. The space of symmetric 2-tensors is denoted by $\mathbb{R}^{3 \times 3}_{\text{sym}}$ and endowed with the natural scalar product $\boldsymbol{\alpha} : \boldsymbol{\beta} := \text{tr}(\boldsymbol{\alpha}\boldsymbol{\beta})$, where $\text{tr}(\boldsymbol{\alpha}) := \alpha_{ii}$, and the corresponding norm $|\boldsymbol{\alpha}|^2 := \boldsymbol{\alpha} : \boldsymbol{\alpha}$. Moreover, $\mathbb{R}^{3 \times 3}_{\text{sym}}$ is orthogonally decomposed into $\mathbb{R}^{3 \times 3}_{\text{sym}} = \mathbb{R}^{3 \times 3}_{\text{dev}} \oplus \mathbb{R} \, \mathbf{1}_2$, where $\mathbb{R} \, \mathbf{1}_2$ is the subspace spanned by the identity 2-tensor $\mathbf{1}_2$ and $\mathbb{R}^{3 \times 3}_{\text{dev}}$ is the subspace of deviatoric (trace-free) symmetric tensors. In particular, for all $\boldsymbol{\alpha} \in \mathbb{R}^{3 \times 3}_{\text{sym}}$, we have the decomposition $\boldsymbol{\alpha} = \text{dev} \, \boldsymbol{\alpha} + (\text{tr} \, \boldsymbol{\alpha})\mathbf{1}_2/3$.

2.2. State variables

Let $\boldsymbol{u} : \Omega \to \mathbb{R}^3$ be the displacement from the reference configuration $\Omega \subset \mathbb{R}^3$ of the body. Moving within the small-deformation regime, we additively decompose the linearized strain $\boldsymbol{\varepsilon} = \boldsymbol{\varepsilon}(\boldsymbol{u}) = (\nabla \boldsymbol{u} + \nabla \boldsymbol{u}^\top)/2$ as

$$\boldsymbol{\varepsilon} = \boldsymbol{\varepsilon}^{\text{el}} + \boldsymbol{e}^{\text{tr}}.$$

Here, $\boldsymbol{\varepsilon}^{\mathrm{el}} = \mathbb{C}^{-1}\boldsymbol{\sigma} \subset \mathbb{R}^{3\times 3}_{\mathrm{sym}}$ corresponds to the elastic part of the strain, $\mathbb{C}$ is the isotropic elasticity tensor, and $\boldsymbol{\sigma}$ is the stress. The tensor $\boldsymbol{e}^{\mathrm{tr}} \in \mathbb{R}^{3\times 3}_{\mathrm{dev}}$ is the inelastic strain originating from the martensitic transformation and reorientation. In particular, $\boldsymbol{e}^{\mathrm{tr}}$ is assumed to be trace-free, as experiments suggest that martensitic transformations are approximately isochoric. The quantity $|\boldsymbol{e}^{\mathrm{tr}}|$ serves as a measure of the martensitic content of the specimen and fulfills $|\boldsymbol{e}^{\mathrm{tr}}| \leq \epsilon_L$ where ϵ_L is the maximal strain which is obtainable by martensitic reorientation. On the other hand, $\boldsymbol{e}^{\mathrm{tr}}/|\boldsymbol{e}^{\mathrm{tr}}|$ is an indicator of the local orientation of martensites. We shall indicate the absolute temperature of the medium by θ.

2.3. Free energy

The equilibrium of the medium is described by the *free-energy* density

$$\psi(\boldsymbol{\varepsilon}, \boldsymbol{e}^{\mathrm{tr}}, \theta) := c\theta(1 - \log\theta) + \frac{1}{2}(\boldsymbol{\varepsilon} - \boldsymbol{e}^{\mathrm{tr}}) : \mathbb{C}(\boldsymbol{\varepsilon} - \boldsymbol{e}^{\mathrm{tr}}) + \frac{H}{2}|\boldsymbol{e}^{\mathrm{tr}}|^2 + f(\theta)|\boldsymbol{e}^{\mathrm{tr}}| + I(\boldsymbol{e}^{\mathrm{tr}}).$$

The parameter $c > 0$ stands for heat capacity density and scales the purely caloric part of the free energy. The quadratic terms in ψ correspond to the free-energy of linearized elastoplasticity with linear kinematic hardening. In particular, H is a hardening parameter and we are making the simplifying assumption that austenite and martensite present the same elastic response. The last two terms in ψ are instead specific of the SMA model. The value $f(\theta)$ corresponds to the martensite-to-austenite equilibrium stress at temperature θ. A specific form for the function f is introduced in Section 2.5. Let us remark that the only term responsible for the thermomechanical coupling is $f(\theta)|\boldsymbol{e}^{\mathrm{tr}}|$. In particular, we are neglecting here thermal expansion as this appears often to be small in applications. Finally, $I : \mathbb{R}^{3\times 3}_{\mathrm{dev}} \to [0, \infty]$ is the indicator function of the set $\{|\boldsymbol{e}^{\mathrm{tr}}| \leq \epsilon_L\}$ that is $I(\boldsymbol{e}^{\mathrm{tr}}) = 0$ if $|\boldsymbol{e}^{\mathrm{tr}}| \leq \epsilon_L$ and $I(\boldsymbol{e}^{\mathrm{tr}}) = \infty$ otherwise. In particular, the constraint $|\boldsymbol{e}^{\mathrm{tr}}| \leq \epsilon_L$ is enforced at all finite energies.

As the transformation strain $\boldsymbol{e}^{\mathrm{tr}}$ is deviatoric, it is convenient to express the free energy in terms of the decomposition $\boldsymbol{\varepsilon} = (v/3)\mathbf{1}_2 + \boldsymbol{e}$ where $v = \mathrm{tr}\,\boldsymbol{\varepsilon}$ is the volumetric strain and $\boldsymbol{e} = \mathrm{dev}\,\boldsymbol{\varepsilon}$ is the deviatoric strain, respectively. In particular, we have

$$\psi = \psi(v, \boldsymbol{e}, \boldsymbol{e}^{\mathrm{tr}}, \theta) = c\theta(1 - \log\theta) + \frac{K}{2}v^2 + G|\boldsymbol{e} - \boldsymbol{e}^{\mathrm{tr}}|^2 + \frac{H}{2}|\boldsymbol{e}^{\mathrm{tr}}|^2 + f(\theta)|\boldsymbol{e}^{\mathrm{tr}}| + I(\boldsymbol{e}^{\mathrm{tr}})$$

where $K, G > 0$ are here the bulk and the shear modulus, respectively.

2.4. Constitutive relations

We classically obtain the constitutive relations from the variations of the free energy with respect to its variables. In particular, we have that the pressure p, the deviatoric stress $\boldsymbol{s}$ (so that, in particular, we can compute the Cauchy stress as: $\boldsymbol{\sigma} = p\mathbf{1}_2 + \boldsymbol{s}$), the entropy density s, and the thermodynamic variable X associated to the internal variable $\boldsymbol{e}^{\mathrm{tr}}$ read

$$p = \partial_\theta \psi = Kv, \tag{2.1}$$

$$\boldsymbol{s} = \partial_{\boldsymbol{e}} \psi = 2G(\boldsymbol{e} - \boldsymbol{e}^{\mathrm{tr}}), \tag{2.2}$$

$$s = -\partial_\theta \psi = -f'(\theta)|\boldsymbol{e}^{\mathrm{tr}}| + c\log\theta - c, \tag{2.3}$$

$$X = -\partial_{\boldsymbol{e}^{\mathrm{tr}}} \psi = \boldsymbol{s} - H\boldsymbol{e}^{\mathrm{tr}} - f(\theta)\partial|\boldsymbol{e}^{\mathrm{tr}}| - \partial I(\boldsymbol{e}^{\mathrm{tr}}). \tag{2.4}$$

Here and in the following we use the symbol ∂ either to indicate classical partial differentiation (in the smooth case) or subdifferentiation in the sense of convex analysis (in the nonsmooth but convex case). In particular, we explicitly record that

$$\partial|\boldsymbol{e}^{\mathrm{tr}}| = \begin{cases} \dfrac{\boldsymbol{e}^{\mathrm{tr}}}{|\boldsymbol{e}^{\mathrm{tr}}|} \text{if } \boldsymbol{e}^{\mathrm{tr}} \neq \mathbf{0}, \\ \{|\boldsymbol{e}^{\mathrm{tr}}| \leq 1\} \quad \text{if } \boldsymbol{e}^{\mathrm{tr}} = \mathbf{0}, \end{cases}$$

$$\partial I(\boldsymbol{e}^{\mathrm{tr}}) = \begin{cases} \mathbf{0} & \text{if } |\boldsymbol{e}^{\mathrm{tr}}| < \epsilon_L, \\ \xi\dfrac{\boldsymbol{e}^{\mathrm{tr}}}{|\boldsymbol{e}^{\mathrm{tr}}|}, & \xi \geq 0 \quad \text{if } |\boldsymbol{e}^{\mathrm{tr}}| = \epsilon_L, \\ \emptyset & \text{if } |\boldsymbol{e}^{\mathrm{tr}}| > \epsilon_L. \end{cases}$$

Moreover, we will also use the convention $\partial\mathcal{S} = -\partial(-\mathcal{S})$ for a concave $\mathcal{S}$.

The internal energy density u can be classically computed as

$$u = u(\boldsymbol{\varepsilon}, \boldsymbol{e}^{\mathrm{tr}}, \theta) = \psi + \theta s$$
$$= c\theta + \frac{K}{2}v^2 + G|\boldsymbol{e} - \boldsymbol{e}^{\mathrm{tr}}|^2 + (f(\theta) - \theta f'(\theta))|\boldsymbol{e}^{\mathrm{tr}}| + \frac{H}{2}|\boldsymbol{e}^{\mathrm{tr}}|^2 + I(\boldsymbol{e}^{\mathrm{tr}}). \tag{2.5}$$

2.5. Choice of f

As mentioned above, the value $f(\theta)$ indicates the martensite–austenite transformation stress at temperature θ. In particular, $f = 0$ for low temperatures and $f' = \beta > 0$ for large temperatures. The transition between these two regimes takes place in a neighborhood of the martensite-to-austenite transition temperature at zero stress θ_{tr}. For the sake of definiteness, in the following we specifically choose the function

$$f(\theta) = \begin{cases} 0 & \text{for } \theta < \theta_{\mathrm{tr}} - \rho \\ \dfrac{\beta}{4\rho}(\theta - (\theta_{\mathrm{tr}} - \rho))^2 & \text{for } |\theta - \theta_{\mathrm{tr}}| \leq \rho \\ \beta(\theta - \theta_{\mathrm{tr}}) & \text{for } \theta > \theta_{\mathrm{tr}} + \rho \end{cases}$$

being however intended that other choices would be possible.

Note that f is bounded, together with its first two derivatives. In particular, the upper bound of the second derivative is strictly needed for the thermodynamic consistency of the model. This forces the parameter $\rho > 0$ to be not too small, see below. Indeed, for $\rho \to 0$ one has that $f(\theta) \to \beta(\theta - \theta_{\mathrm{tr}})^+$ uniformly, which is not differentiable. Following the discussion in [21], we shall tacitly assume in all of the following the consistency condition

$$c - \theta f''(\theta)|\boldsymbol{e}^{\mathrm{tr}}| > 0. \tag{2.6}$$

This condition amounts to ensure that $\partial_\theta s = -f''(\theta)|\boldsymbol{e}^{\mathrm{tr}}| + c/\theta > 0$ so that the effective heat capacity of the medium is positive.

Let us anticipate that, along the analysis, the introduction of a smooth truncation of f will be needed and additional constraints on the material parameters will be introduced, namely (4.6), (4.10), and (4.20). These constrains are aimed at ensuring the dissipativity of the system and are to be compared with analogous conditions from [20,21]. Let us explicitly stress that these requirements are compatible with the experimentally observed material parameters, see Table 8.

2.6. Dissipation and flow rule

In order to describe the evolution of the medium we shall prescribe a (pseudo-)potential of *dissipation* D : $\mathbb{R}_+ \times \mathbb{R}^{3\times3}_{\mathrm{dev}} \to [0, \infty)$ of Von-Mises type, namely

$$D(\theta; \dot{\boldsymbol{e}}^{\mathrm{tr}}) := \frac{R}{\theta}|\dot{\boldsymbol{e}}^{\mathrm{tr}}|$$

where $R > 0$ is an activation radius, measured in MPaK. The flow rule consists in the classical normality principle

$$\partial_{\dot{\boldsymbol{e}}^{\mathrm{tr}}} D(\theta; \dot{\boldsymbol{e}}^{\mathrm{tr}}) \ni \frac{\boldsymbol{X}}{\theta}. \tag{2.7}$$

Note that relation (2.7) can be equivalently expressed in the complementary form

$$F(\theta; \boldsymbol{X}) \leq 0, \qquad \dot{\xi} \geq 0, \qquad F(\theta, \boldsymbol{X})\dot{\xi} = 0, \qquad \dot{\boldsymbol{e}}^{\mathrm{tr}} = \dot{\xi}\frac{\partial_{\boldsymbol{X}} F(\theta; \boldsymbol{X})}{|\partial_{\boldsymbol{X}} F(\theta; \boldsymbol{X})|}$$

where the yield function F is defined as

$$F(\theta; \boldsymbol{X}) := |\boldsymbol{X}| - \frac{R}{\theta}.$$

In particular, F is related to D via the duality formula

$$D(\theta; \dot{\boldsymbol{e}}^{\mathrm{tr}}) = \sup\{\boldsymbol{X} : \dot{\boldsymbol{e}}^{\mathrm{tr}} \mid F(\theta; \boldsymbol{X}) \leq 0\}.$$

By combining (2.4) with (2.7) we obtain the constitutive material relation equation

$$\partial_{\dot{e}^{\mathrm{tr}}} D(\theta; \dot{e}^{\mathrm{tr}}) + \partial_{e^{\mathrm{tr}}} \psi(\varepsilon, e^{\mathrm{tr}}, \theta) \ni 0. \tag{2.8}$$

2.7. Momentum balance and energy conservation

Assume that the reference configuration of the body $\Omega \subset \mathbb{R}^3$ is nonempty, open, connected, and has a Lipschitz continuous boundary Γ. We decompose the latter as $\Gamma = \Gamma^D \cap \Gamma^N \cap \partial \Gamma$ where Γ^D and Γ^N are disjoint and relatively open in Γ, $\partial \Gamma$ is the boundary of both Γ^D and Γ^N, and Γ^D has positive surface measure. Given some final reference time $T > 0$, we shall be considering the quasistatic momentum balance

$$\nabla \cdot \sigma + f = 0 \quad \text{in } \Omega \times (0, T) \tag{2.9}$$

to be combined with the boundary conditions

$$\sigma n = g \quad \text{on } \Gamma^N \times (0, T), \qquad u = h \quad \text{on } \Gamma^D \times (0, T). \tag{2.10}$$

Here, n denotes the outward unit normal to Γ^N and $f : \Omega \times (0, T) \to \mathbb{R}^3$ and $g : \Gamma^N \times (0, T) \to \mathbb{R}^3$ are a body force and a surface traction, respectively, while $h : \Gamma^D \times (0, T) \to \mathbb{R}^3$ is a prescribed displacement.

The conservation of energy reads

$$\dot{u} + \nabla \cdot q = \sigma : \dot{\varepsilon} \quad \text{in } \Omega \times (0, T) \tag{2.11}$$

where q represents the heat flux. We shall complement the latter with the homogeneous Neumann boundary conditions

$$q \cdot n = 0 \quad \text{on } \Gamma \times (0, T).$$

Let us however anticipate that different boundary conditions of Robin type will be allowed in the space-homogeneous situation of Section 3.4.

2.8. Full system

The thermomechanical evolution of the medium is described by the system of quasistatic equilibrium (2.9), energy conservation (2.11), and the constitutive material relation (2.8). Along with the current choices for the free energy ψ and the dissipation D, the form of the resulting differential system in terms of the variables $(u, \theta, e^{\mathrm{tr}})$ reads

$$\nabla \cdot \mathbb{C}(\varepsilon(u) - e^{\mathrm{tr}}) + f = 0, \tag{2.12}$$

$$\left(c - \theta f''(\theta) |e^{\mathrm{tr}}|\right) \dot{\theta} + \nabla \cdot q = R|\dot{e}^{\mathrm{tr}}| + \theta f'(\theta) |e^{\mathrm{tr}}|^{\cdot}, \tag{2.13}$$

$$R \partial |\dot{e}^{\mathrm{tr}}| + H e^{\mathrm{tr}} + f(\theta) \partial |e^{\mathrm{tr}}| + \partial I(e^{\mathrm{tr}}) \ni 2G(e(u) - e^{\mathrm{tr}}), \tag{2.14}$$

where we recall that $e(u) := \mathrm{dev}\, \varepsilon(u)$. The thermomechanical coupling depends on the total martensitic content $|e^{\mathrm{tr}}|$. This reflects that the transformation from austenite to martensite is a second-order phase transition whereas the reorientation of martensitic variants is not associated with latent heat production.

2.9. Dissipativity

Let us explicitly comment on the thermodynamic consistency of the model by evaluating the entropy-release-rate density

$$r := \dot{s} + \nabla \cdot Q$$

where $Q := q/\theta$ is the entropy flux. Note preliminarily that energy conservation (2.11) can be equivalently rewritten as

$$\theta \dot{s} + \nabla \cdot q = X : \dot{e}^{\mathrm{tr}}. \tag{2.15}$$

Then, we use (2.15) and (2.7) in order to compute

$$r \overset{(2.15)}{=} \frac{1}{\theta}X : \dot{e}^{\text{tr}} + \nabla \cdot \left(\frac{q}{\theta}\right) - \frac{1}{\theta}\nabla \cdot q = \frac{1}{\theta}X : \dot{e}^{\text{tr}} + q \cdot \nabla\left(\frac{1}{\theta}\right)$$

$$\overset{(2.7)}{=} \partial_{\dot{e}^{\text{tr}}} D(\theta; \dot{e}^{\text{tr}}) : \dot{e}^{\text{tr}} + q \cdot \nabla\left(\frac{1}{\theta}\right) = D(\theta; \dot{e}^{\text{tr}}) + q \cdot \nabla\left(\frac{1}{\theta}\right) \geq 0$$

where the inequality follows from the fact that $D > 0$ whenever $q = \alpha(1/\nabla\theta)$ with α monotone and $\alpha(0) = 0$. For the sake of definiteness we shall let $q = \kappa\nabla(1/\theta)$ for some conductivity $\kappa \geq 0$, this choice being particularly adapted to the present nonisothermal situation, see below. It is however intended that our discussion can be reproduced in greater generality. In particular, the classical Fourier law $q = -\kappa\nabla\theta$ (which actually corresponds to a linearization of $q = \kappa\nabla(1/\theta)$ around some reference temperature) can also be accommodated.

3. Gradient structures

We are now in the position of introducing the generalized-gradient-flow reformulation of the full thermomechanical evolution system presented in the previous section. This corresponds to relation (1.1) along with the choice $y = (e^{\text{tr}}, \theta)$ and the definition of the total entropy

$$S(y) = \int_{\Omega} s(y)\mathrm{d}x = \int_{\Omega} (-f'(\theta)|e^{\text{tr}}| + c\log\theta - c)\mathrm{d}x$$

so that one has

$$\partial S(y) = \begin{pmatrix} -f'(\theta)\partial|e^{\text{tr}}| \\ (c - \theta f''(\theta)|e^{\text{tr}}|)/\theta \end{pmatrix}.$$

To obtain this variational formulation, we start by eliminating the mechanical variable u by solving the equilibrium, for given transformation strain e^{tr} and time t, see Section 3.1. This preliminary step is unavoidable as mechanical equilibrium follows from energy stationarity rather than from entropic effects. The gradient reformulation of resulting thermomechanical problem (2.12) + (2.14) then follows from the choice of the entropy-dissipation potential $\mathcal{K}(t, y; \cdot)$ fulfilling the structural assumption (1.2). By dualizing $\mathcal{K}(t, y; \cdot)$ with respect to the rates, one can equivalently express relation (1.1) as

$$\dot{y} \in \partial_{\xi}\mathcal{K}^*(t, y; \partial S(y)) \tag{3.1}$$

where the *dual-entropy-dissipation potential* $\mathcal{K}^*(t, y; \cdot)$ is a function of the thermodynamic force $\xi = \partial S(y)$.

We start by presenting a reformulation for the isothermal problem in Section 3.2. Then, we consider the general nonisothermal situation in Section 3.3. Finally, in Section 3.4 we tackle the special case of space-homogeneous fields as this is both often close to real applications and a clear benchmark for implementation.

3.1. Resolution of the quasistatic equilibrium

The first step in the direction of a variational reformulation of the system (2.12)–(2.14) consists in expressing u in terms of e^{tr} and external actions by solving the quasistatic mechanical equilibrium system. Indeed, for all $e^{\text{tr}} \in L^2(\Omega; \mathbb{R}^{3\times3}_{\text{dev}}), f(t) \in L^2(\Omega; \mathbb{R}^3)$, and $g(t) \in L^2(\Gamma^{\text{tr}}; \mathbb{R}^3)$ one can find a unique $u \in \mathcal{U} := H^1(\Omega; \mathbb{R}^3)$ solving (2.9)–(2.10). We shall indicate such u as $\widehat{u}(t, e^{\text{tr}})$. Given $(f, g) \in C([0, T], L^2(\Omega; \mathbb{R}^3) \times L^2(\Gamma^{\text{tr}}; \mathbb{R}^3))$, the solution operator $\widehat{u} : [0, T] \times L^2(\Omega; \mathbb{R}^{3\times3}_{\text{sym}}) \rightarrow \mathcal{U}$ is hence well-defined, linear in e^{tr}, and continuous in (t, e^{tr}), although nonlocal in space. The latter solution operator $\widehat{u}$ will be systematically employed in the remainder of the paper.

Note that by assuming $\widehat{u}$ to be independent of time (that is, f, g, and h to be independent of time) we deduce that $\varepsilon(\widehat{u}(e^{\text{tr}}))$ coincides with e^{tr} up to a linear shift. In this case (which, strictly speaking, is the only one covered by the original GENERIC theory, which presently does not allow external actions) the evolution of the material is driven solely by temperature relaxation.

3.2. Gradient structure of the isothermal problem

Let us firstly concentrate on the *isothermal* problem (2.12) + (2.14). This can be written in the general form (1.1) by defining $\boldsymbol{y} = \boldsymbol{e}^{\mathrm{tr}}$ and

$$\mathcal{K}^*(t, \boldsymbol{y}; \boldsymbol{\xi}) := \int_{\Omega} I_{R/\theta}(\boldsymbol{\xi} - \boldsymbol{b}(t, \boldsymbol{y})) \mathrm{d}x$$

where $I_{R/\theta}$ is the indicator function of the convex set $\{\boldsymbol{a} \in \mathbb{R}^{3 \times 3}_{\mathrm{dev}} : |\boldsymbol{a}| \le R/\theta\}$ and we used the short-hand notation

$$\boldsymbol{b}(t, \boldsymbol{y}) \in \frac{1}{\theta} \left(-2G(\boldsymbol{e}(\widehat{\boldsymbol{u}}(t, \boldsymbol{e}^{\mathrm{tr}})) - \boldsymbol{e}^{\mathrm{tr}}) + H\boldsymbol{e}^{\mathrm{tr}} + (f(\theta) - \theta f'(\theta)) \partial |\boldsymbol{e}^{\mathrm{tr}}| + \partial I(\boldsymbol{e}^{\mathrm{tr}}) \right)$$

for the purely state-dependent nonlinear operator $\boldsymbol{b}$, which is continuous in time. The above-defined dual-entropy production potential $\boldsymbol{\xi} \mapsto \mathcal{K}^*(t, \boldsymbol{y}; \boldsymbol{\xi})$ is clearly convex. By computing its dual we get

$$\mathcal{K}(t, \boldsymbol{y}; \dot{\boldsymbol{y}}) = \int_{\Omega} \frac{R}{\theta} |\dot{\boldsymbol{e}}^{\mathrm{tr}}| \mathrm{d}x + \int_{\Omega} \boldsymbol{b}(t, \boldsymbol{y}) : \dot{\boldsymbol{e}}^{\mathrm{tr}} \mathrm{d}x$$

which obviously fulfills the convexity assumption (1.2).

The above choices for $\mathcal{S}$ and $\mathcal{K}$ entail a reformulation of the isothermal evolution in terms of (1.1). Note nonetheless that the isothermal case can be also classically formulated as the gradient flow in the variables $(\boldsymbol{u}, \boldsymbol{e}^{\mathrm{tr}})$ of the complementary energy

$$\Psi(t; \boldsymbol{u}, \boldsymbol{e}^{\mathrm{tr}}) := \int_{\Omega} \left(\frac{1}{2}(\boldsymbol{\varepsilon}(\boldsymbol{u}) - \boldsymbol{e}^{\mathrm{tr}}) : \mathbb{C}(\boldsymbol{\varepsilon}(\boldsymbol{u}) - \boldsymbol{e}^{\mathrm{tr}}) + \frac{H}{2}|\boldsymbol{e}^{\mathrm{tr}}|^2 + f(\theta)|\boldsymbol{e}^{\mathrm{tr}}| + I(\boldsymbol{e}^{\mathrm{tr}}) \right) \mathrm{d}x$$
$$- \int_{\Omega} \boldsymbol{f}(t) \cdot \boldsymbol{u} \mathrm{d}x - \int_{\Gamma^{\mathrm{tr}}} \boldsymbol{g}(t) \cdot \boldsymbol{u} \mathrm{d}\Gamma$$

subject to the Von Mises dissipative potential

$$\mathcal{D}(\dot{\boldsymbol{u}}, \dot{\boldsymbol{e}}^{\mathrm{tr}}) := R|\dot{\boldsymbol{e}}^{\mathrm{tr}}|.$$

Indeed, the system (2.12) + (2.14) (along with boundary conditions) corresponds to the relation

$$\partial \mathcal{D}(\dot{\boldsymbol{u}}, \dot{\boldsymbol{e}}^{\mathrm{tr}}) + \partial \Psi(t; \boldsymbol{u}, \boldsymbol{e}^{\mathrm{tr}}) \ni 0$$

which is indeed formally close to (1.1). By solving for $\boldsymbol{u} = \widehat{\boldsymbol{u}}(t, \boldsymbol{e}^{\mathrm{tr}})$ one can additionally reformulate the latter in the sole variable $\boldsymbol{e}^{\mathrm{tr}}$ (and time) as

$$\partial R|\dot{\boldsymbol{e}}^{\mathrm{tr}}| + \partial_{\boldsymbol{e}^{\mathrm{tr}}} \Psi(t; \widehat{\boldsymbol{u}}(t, \boldsymbol{e}^{\mathrm{tr}}), \boldsymbol{e}^{\mathrm{tr}}) \ni 0.$$

Note that the latter equation, although local in space and time, features the nonlocal-in-space operator $\widehat{\boldsymbol{u}}$.

3.3. Gradient structure in the general case

In the general nonisothermal case we can follow [16, Sec. 3.4] and recast the evolution problem in the form of (3.1) by letting the dual entropy-production potential be defined by

$$\mathcal{K}^*(t, \boldsymbol{y}; \boldsymbol{\xi}) = \int_{\Omega} I_{R/\theta}(\boldsymbol{\xi}_1 - \boldsymbol{a}(t, \boldsymbol{y})\xi_2) \mathrm{d}x + \int_{\Omega} \frac{\kappa}{2} \left| \frac{\nabla \xi_2}{\gamma(\boldsymbol{y})} \right|^2 \mathrm{d}x \tag{3.2}$$

for $\boldsymbol{\xi} = (\boldsymbol{\xi}_1, \xi_2) \in L^2(\Omega; \mathbb{R}^{3 \times 3}_{\mathrm{sym}}) \times L^2(\Omega)$ where we have denoted by

$$\gamma(\boldsymbol{y}) := c - \theta f''(\theta)|\boldsymbol{e}^{\mathrm{tr}}|$$
$$\boldsymbol{a}(t, \boldsymbol{y}) \in \frac{1}{\gamma(\boldsymbol{y})}(-2G(\boldsymbol{e}(\widehat{\boldsymbol{u}}(t, \boldsymbol{e}^{\mathrm{tr}})) - \boldsymbol{e}^{\mathrm{tr}}) + H\boldsymbol{e}^{\mathrm{tr}} + (f(\theta) - \theta f'(\theta)) \partial |\boldsymbol{e}^{\mathrm{tr}}| + \partial I(\boldsymbol{e}^{\mathrm{tr}})).$$

In this case, we can compute

$$\partial_{\boldsymbol{\xi}} \mathcal{K}^*(t, \boldsymbol{y}; \boldsymbol{\xi}) \supset \begin{pmatrix} \partial I_{R/\theta}(\boldsymbol{\xi}_1 - \boldsymbol{a}(t, \boldsymbol{y})\xi_2) \\ -\partial I_{R/\theta}(\boldsymbol{\xi}_1 - \boldsymbol{a}(t, \boldsymbol{y})\xi_2) : \boldsymbol{a}(t, \boldsymbol{y}) - \dfrac{\kappa}{(\gamma(\boldsymbol{y}))^2}\Delta \xi_2 \end{pmatrix}$$

so that, by substituting

$$\boldsymbol{\xi} \in \partial \mathcal{S}(\boldsymbol{y}) = \begin{pmatrix} -f'(\theta)\partial|\boldsymbol{e}^{\mathrm{tr}}| \\ \dfrac{\gamma(\boldsymbol{y})}{\theta} \end{pmatrix}$$

one gets

$$\partial_{\boldsymbol{\xi}} \mathcal{K}^*(t, \boldsymbol{y}; \partial \mathcal{S}(\boldsymbol{y})) \supset \begin{pmatrix} \partial I_{R/\theta}\left(-f'(\theta)\partial|\boldsymbol{e}^{\mathrm{tr}}| - \boldsymbol{a}(t, \boldsymbol{y})\dfrac{\gamma(\boldsymbol{y})}{\theta}\right) \\ -\partial I_{R/\theta}\left(-f'(\theta)\partial|\boldsymbol{e}^{\mathrm{tr}}| - \boldsymbol{a}(t, \boldsymbol{y})\dfrac{\gamma(\boldsymbol{y})}{\theta}\right) : \boldsymbol{a}(t, \boldsymbol{y}) - \dfrac{\kappa}{\gamma(\boldsymbol{y})}\Delta\left(\dfrac{1}{\theta}\right) \end{pmatrix}.$$

By using the above-introduced expressions for $\boldsymbol{a}$ and γ one obtains that the argument of the subdifferential $\partial I_{R/\theta}$ is nothing but $-X/\theta$ so that (3.1) reads

$$\begin{pmatrix} \dot{\boldsymbol{e}}^{\mathrm{tr}} \\ \dot{\theta} \end{pmatrix} \in \begin{pmatrix} \partial I_{R/\theta}(X/\theta) \\ -\partial I_{R/\theta}(X/\theta) : \boldsymbol{a}(t, \boldsymbol{y}) - \dfrac{\kappa}{\gamma(\boldsymbol{y})}\Delta\left(\dfrac{1}{\theta}\right) \end{pmatrix}$$

corresponding indeed to relations (2.13)–(2.14).

By computing the dual of $\mathcal{K}^*(t, \boldsymbol{y}; \cdot)$ one obtains the entropy-production potential

$$\mathcal{K}(t, \boldsymbol{y}; \dot{\boldsymbol{y}}) = \int_{\Omega} \frac{R}{\theta}|\dot{\boldsymbol{e}}^{\mathrm{tr}}|\mathrm{d}x + \frac{1}{2\kappa}\|\gamma(\boldsymbol{y})(\dot{\theta} + \boldsymbol{a}(t, \boldsymbol{y}) : \dot{\boldsymbol{e}}^{\mathrm{tr}})\|^2_{H^{-1}_{\mathrm{av}}} \tag{3.3}$$

featuring the norm

$$\|v\|^2_{H^{-1}_{\mathrm{av}}} := \int_{\Omega} |\nabla(-\Delta^{-1}v)|^2\mathrm{d}x = \int_{\Omega} |\nabla w|^2\mathrm{d}x.$$

Here, w is the unique solution in

$$H^1_{\mathrm{av}} := \left\{ w \in H^1(\Omega) : \int_{\Omega} w\,\mathrm{d}x = 0 \right\}$$

of $-\Delta w = v$ for

$$v \in H^{-1}_{\mathrm{av}} := \left\{ v \in H^{-1}(\Omega) : \langle v, 1 \rangle = 0 \right\}$$

where $\langle \cdot, \cdot \rangle$ stands for the duality pairing between $H^{-1}(\Omega)$ and $H^1(\Omega)$. Note that $\mathcal{K}(t, \boldsymbol{y}, \cdot)$ fulfills the general structural assumption (1.2).

We hence compute

$$\partial_{\dot{\boldsymbol{y}}} \mathcal{K}(t, \boldsymbol{y}; \dot{\boldsymbol{y}}) \supset \begin{pmatrix} \dfrac{R}{\theta}\partial|\dot{\boldsymbol{e}}^{\mathrm{tr}}| + \dfrac{\gamma(\boldsymbol{y})}{\kappa}(-\Delta^{-1})(\gamma(\boldsymbol{y})(\dot{\theta} + \boldsymbol{a}(t, \boldsymbol{y}) : \dot{\boldsymbol{e}}^{\mathrm{tr}}))\boldsymbol{a}(t, \boldsymbol{y}) \\ \dfrac{\gamma(\boldsymbol{y})}{\kappa}(-\Delta^{-1})(\gamma(\boldsymbol{y})(\dot{\theta} + \boldsymbol{a}(t, \boldsymbol{y}) : \dot{\boldsymbol{e}}^{\mathrm{tr}})) \end{pmatrix}.$$

By substituting $\partial \mathcal{S}(\boldsymbol{y})$ into (1.1) we obtain

$$\begin{pmatrix} \dfrac{R}{\theta}\partial|\dot{\boldsymbol{e}}^{\mathrm{tr}}| + \dfrac{\gamma(\boldsymbol{y})}{\kappa}(-\Delta^{-1})(\gamma(\boldsymbol{y})(\dot{\theta} + \boldsymbol{a}(t, \boldsymbol{y}) : \dot{\boldsymbol{e}}^{\mathrm{tr}}))\boldsymbol{a}(t, \boldsymbol{y}) \\ \dfrac{\gamma(\boldsymbol{y})}{\kappa}(-\Delta^{-1})(\gamma(\boldsymbol{y})(\dot{\theta} + \boldsymbol{a}(t, \boldsymbol{y}) : \dot{\boldsymbol{e}}^{\mathrm{tr}})) \end{pmatrix} - \begin{pmatrix} -f'(\theta)\partial|\boldsymbol{e}^{\mathrm{tr}}| \\ \dfrac{\gamma(\boldsymbol{y})}{\theta} \end{pmatrix} \ni \begin{pmatrix} \boldsymbol{0} \\ 0 \end{pmatrix}$$

and relations (2.13)–(2.14) follow from the actual choices of $\boldsymbol{a}$ and γ. Note that the argument of the H^{-1}-norm above is required to have zero mean. Given the equation for θ, this amounts to say that $\boldsymbol{q} = \kappa\nabla(1/\theta)$ has no flux through the boundary Γ. Namely, the body is assumed to be thermally insulated from the exterior.

3.4. Gradient structures for space-homogeneous fields

We shall be here concerned with some specific degenerate case in which the energy conservation equation (2.13) can be actually reduced to an ordinary differential relation. In particular, we assume that the temperature is constant in space. This can be regarded as a sensible approximation in many applicative instances, especially in connection with relatively thin structures activated at low frequencies. The advantage of this approximation is that the energy conservation equation (2.13) is pointwise in space and time. In particular, by dropping the differential term in (2.13) one gets

$$\left(c - \theta f''(\theta)|\boldsymbol{e}^{\mathrm{tr}}|\right)\dot{\theta} = R|\dot{\boldsymbol{e}}^{\mathrm{tr}}| + \theta f'(\theta)|\boldsymbol{e}^{\mathrm{tr}}|\cdot \tag{3.4}$$

which can be seen as the entropy gradient flow driven by the entropy-production potential

$$\mathcal{K}(t, \boldsymbol{y}; \dot{\boldsymbol{y}}) = \begin{cases} \displaystyle\int_\Omega \frac{R}{\theta}|\dot{\boldsymbol{e}}^{\mathrm{tr}}|\mathrm{d}x & \text{if } \gamma(\boldsymbol{y})(\dot{\theta} + \boldsymbol{a}(t, \boldsymbol{y}) : \dot{\boldsymbol{e}}^{\mathrm{tr}}) = 0, \\ \infty & \text{otherwise.} \end{cases}$$

Note that this choice of $\mathcal{K}$ formally corresponds to the limit as $\kappa \to 0$ in (3.3). In particular, it translates at the variational level the situation where the term $\kappa\Delta(1/\theta)$ in (2.13) is dropped by letting $\kappa \to 0$. The reduced energy-conservation relation (2.13) reads in this case

$$\gamma(\boldsymbol{y})(\dot{\theta} + \boldsymbol{a}(t, \boldsymbol{y}) : \dot{\boldsymbol{e}}^{\mathrm{tr}}) = 0$$

and is directly enforced as a constraint in the definition of $\mathcal{K}$.

One can extend the above discussion by including a relaxation dynamics for the temperature. Indeed, by replacing $\kappa\Delta(1/\theta)$ by $-\lambda/\theta$ in (2.13) one gets

$$\left(c - \theta f''(\theta)|\boldsymbol{e}^{\mathrm{tr}}|\right)\dot{\theta} - \frac{\lambda}{\theta} = R|\dot{\boldsymbol{e}}^{\mathrm{tr}}| + \theta f'(\theta)|\boldsymbol{e}^{\mathrm{tr}}|\cdot \tag{3.5}$$

corresponding indeed to a viscous flow. Note that this approximation can be made rigorous by assuming all fields to be space-homogeneous and integrating (2.13) in space with the aid of the Robin-type boundary condition

$$\boldsymbol{q} \cdot \boldsymbol{n} = -\frac{\widehat{\lambda}}{\theta}$$

where $\widehat{\lambda} = \lambda|\Omega|/|\Gamma|$, being $|\Gamma|$ and $|\Omega|$ the measures of Γ and Ω, respectively. This case corresponds to the gradient flow of the entropy driven by the dual-entropy-production potential (compare with (3.2))

$$\mathcal{K}^*(t, \boldsymbol{y}; \boldsymbol{\xi}) = \int_\Omega I_{R/\theta}(\boldsymbol{\xi}_1 - \boldsymbol{a}(t, \boldsymbol{y})\xi_2)\mathrm{d}x + \int_\Omega \frac{\lambda}{2}\left|\frac{\xi_2}{\gamma(\boldsymbol{y})}\right|^2\mathrm{d}x \tag{3.6}$$

and, correspondingly, the entropy-production potential

$$\mathcal{K}(t, \boldsymbol{y}; \dot{\boldsymbol{y}}) = \int_\Omega \frac{R}{\theta}|\dot{\boldsymbol{e}}^{\mathrm{tr}}|\mathrm{d}x + \int_\Omega \frac{1}{2\lambda}|\gamma(\boldsymbol{y})(\dot{\theta} + \boldsymbol{a}(t, \boldsymbol{y}) : \dot{\boldsymbol{e}}^{\mathrm{tr}})|^2\mathrm{d}x. \tag{3.7}$$

Note that the above entropy potential features no differentiation terms with respect to space and fulfills the structural assumption (1.2).

We are in the position of generalizing the choice of the boundary condition even further and let the system adapt to some given external temperature. In particular, this amounts in asking for

$$\boldsymbol{q} \cdot \boldsymbol{n} = \widehat{\lambda}\left(\frac{1}{\theta^e(t)} - \frac{1}{\theta}\right)$$

for some possibly time-dependent external temperature $t \mapsto \theta^e(t) > 0$. By assuming space-homogeneity, one replaces (2.13) with the ordinary differential equation

$$\left(c - \theta f''(\theta)|e^{\mathrm{tr}}|\right)\dot{\theta} + \lambda\left(\frac{1}{\theta^e(t)} - \frac{1}{\theta}\right) = R|\dot{e}^{\mathrm{tr}}| + \theta f'(\theta)|e^{\mathrm{tr}}|^{\cdot}. \tag{3.8}$$

Then, the system (2.14) + (3.8) corresponds to the choice

$$\mathcal{K}^*(t, \mathbf{y}; \boldsymbol{\xi}) = I_{R/\theta}(\xi_1 - \mathbf{a}\xi_2) + \frac{\widehat{\lambda}}{2}\left|\frac{\xi_2}{\gamma(\mathbf{y})} - \frac{1}{\theta_e(t)}\right|^2 + \frac{1}{\theta^e(t)}\left(\frac{\xi_2}{\gamma(\mathbf{y})} - \frac{1}{\theta^e(t)}\right).$$

By duality we obtain the time-dependent entropy-production potential

$$\mathcal{K}(t, \mathbf{y}, \dot{\mathbf{y}}) = \frac{R}{\theta}|\dot{e}^{\mathrm{tr}}| + \frac{1}{2\widehat{\lambda}}|\gamma(\mathbf{y})(\dot{\theta} + \mathbf{a}(t, \mathbf{y}) : \dot{e}^{\mathrm{tr}})|^2 + \frac{\gamma(\mathbf{y})}{\theta^e(t)}(\dot{\theta} + \mathbf{a}(t, \mathbf{y}) : \dot{e}^{\mathrm{tr}})$$

which again fulfills the basic assumption (1.2). By computing (1.1) in this case one obtains in particular (3.8). One has to mention that the corresponding system cannot be regarded to be closed, as the external temperature θ^e provides an entropic source.

4. Semi-implicit scheme for the space-homogeneous case

The gradient flow structure of the model may be used to derive and analyze some dissipative numerical scheme. We shall detail this possibility by focusing here on the space-homogeneous case of relations (3.8) + (2.14), which equivalently read

$$\gamma(\mathbf{y})\left(\dot{\theta} + \mathbf{a}(t, \mathbf{y}) : \dot{e}^{\mathrm{tr}}\right) + \lambda\left(\frac{1}{\theta_{\mathrm{ext}}(t)} - \frac{1}{\theta}\right) = 0, \tag{4.1}$$

$$\frac{R}{\theta}\partial|\dot{e}^{\mathrm{tr}}| + \frac{\gamma(\mathbf{y})}{\theta}\mathbf{a}(t, \mathbf{y}) + f'(\theta)\partial|e^{\mathrm{tr}}| \ni 0 \tag{4.2}$$

where we recall that

$$\gamma(\mathbf{y}) = c - \theta f''(\theta)|e^{\mathrm{tr}}|$$

$$\mathbf{a}(t, \mathbf{y}) \in \frac{1}{\gamma(\mathbf{y})}\left(-2G(e(\widehat{\mathbf{u}}(t, e^{\mathrm{tr}})) - e^{\mathrm{tr}}) + He^{\mathrm{tr}} + (f(\theta) - \theta f'(\theta))\partial|e^{\mathrm{tr}}| + \partial I(e^{\mathrm{tr}})\right).$$

This approximation of the original system, indeed justified for space-homogeneous fields, bears a particular interest as it is space-localized and even rate-independent, for $\lambda = 0$. We hence believe this to be a relevant test case. PDE couplings will be investigated in a forthcoming paper.

We are interested in a semi-implicit time-discretization scheme. Let a time-partition $\{0 = t_0 < t_1 < \cdots < t_N = T\}$ be given and define the possibly variable time step $\tau_i = t_i - t_{i-1}$. We focus here on the strain- and external-temperature-driven setting. In particular, we assume to be given $t \in [0, T] \mapsto e(t) := \mathrm{dev}\,\boldsymbol{\varepsilon}(\mathbf{u}(t)) \in \mathbb{R}^{3\times3}_{\mathrm{dev}}$ and $t \in [0, T] \mapsto \theta^e(t) > 0$ and a suitable initial conditions on $e_0^{\mathrm{tr}} \in \mathbb{R}^{3\times3}_{\mathrm{dev}}$ and $\theta_0 > 0$, and we are interested in the time-discrete scheme

$$\gamma_\eta(\mathbf{y}_{i-1})\left(\frac{\theta_i - \theta_{i-1}}{\tau_i} + \mathbf{a}_\eta(t_i, \mathbf{y}_i) : \frac{e_i^{\mathrm{tr}} - e_{i-1}^{\mathrm{tr}}}{\tau_i}\right) + \tau_i\lambda\left(\frac{1}{\theta^e(t_i)} - \frac{1}{\theta_i}\right) = 0, \tag{4.3}$$

$$\frac{R}{\theta_i}\partial|e_i^{\mathrm{tr}} - e_{i-1}^{\mathrm{tr}}| + \frac{\gamma_\eta(\mathbf{y}_{i-1})}{\theta_i}\mathbf{a}_\eta(t_i, \mathbf{y}_i) + f'_*(\theta_i)\partial|e_i^{\mathrm{tr}}|_\eta \ni 0, \tag{4.4}$$

where the state dependence is explicit in γ and implicit everywhere else. The variational structure of (4.1)–(4.2) is indeed reflected in this choice, as all occurrences of γ are likewise discretized. Additionally, for the purpose of presenting a complete theoretical analysis of the scheme, we are forced to perform a regularization of the thermomechanical coupling term $f(\theta)|e^{\mathrm{tr}}|$ by $f_*(\theta)|e^{\mathrm{tr}}|_\eta$. Here,

$$|e^{\mathrm{tr}}|_\eta := \min\left\{\frac{|e^{\mathrm{tr}}|^2}{2\eta} + \frac{\eta}{2}, |e^{\mathrm{tr}}|\right\}$$

where $\eta > 0$ is a small used-defined parameter (the modification f^* of f is described below). By reflecting the variational structure of the problem, this regularization entails modifications on the terms γ and $\boldsymbol{a}$ as follows

$$\gamma_\eta(\boldsymbol{y}) := c - \theta f''_*(\theta)|\boldsymbol{e}^{\mathrm{tr}}|_\eta$$

$$\boldsymbol{a}_\eta(t, \boldsymbol{y}) \in \frac{1}{\gamma(\boldsymbol{y})}(-2G(\boldsymbol{e}(t) - \boldsymbol{e}^{\mathrm{tr}}) + H\boldsymbol{e}^{\mathrm{tr}} + (f_*(\theta) - \theta f'_*(\theta))\partial|\boldsymbol{e}^{\mathrm{tr}}|_\eta + \partial I(\boldsymbol{e}^{\mathrm{tr}})).$$

The purpose of the regularization is to ensure that

$$\partial|\boldsymbol{e}^{\mathrm{tr}}|_\eta = (\eta\mathbf{1}_2 + \partial I)^{-1}(\boldsymbol{e}^{\mathrm{tr}}) \tag{4.5}$$

is Lipschitz continuous of constant $1/\eta$, which turns out crucial for proving the convergence of the numerical scheme. Note that $|\partial|\boldsymbol{e}^{\mathrm{tr}}|_\eta| \leq 1$ for all $\boldsymbol{e}^{\mathrm{tr}} \in \mathbb{R}^{3\times3}_{\mathrm{dev}}$. On the other hand, let us mention that the modification is performed *at the functional level*, namely without perturbing the variational structure of the problem. We shall also mention that analogous regularizations have been already considered for this problem [17,18,50] and proved to be consistent with their limit $\eta \to 0$ and that the numerical scheme performs well in the case $\eta = 0$, despite the absence of a complete analysis. We collect some comment in this direction in Section 5.

As for the modified function f_* we simply prescribe a monotone smooth truncation so that $f_* \equiv f$ for $\theta \leq \theta_* - 2\rho$, $f'_* = 0$ for $\theta \geq \theta_*$, and $\|f'_*\|_{L^\infty} := \sup_{\theta>0}|f'_*(\theta)| \leq \beta$, and $\|f''_*\|_{L^\infty} \leq \beta/(2\rho)$ so that (4.6) holds. In particular, $\theta_* > 0$ is some prescribed maximal temperature. This modification with respect to the original f is essentially immaterial with respect to applications, for it suffices to choose θ_* larger than the experimentally observed and computationally simulated temperatures. The temperature upper bound, combined with a compatibility assumption on the parameter, see (4.20), ensures that the overall behavior of the system remains dissipative under cyclic testing. In the context of the Souza–Auricchio model a similar although weaker assumption has been advanced in [21]. The situation was there simpler as the constitutive relation of the material was taken to be scalar and an order method could be used.

We shall prove that the system (4.3)–(4.4) admits a solution for all i. This will be done in Section 4.3 by means of a fixed point argument based on the iterative solution of (4.3) and (4.4). In order to prepare for this, we discuss separately the mechanical and the thermal subproblems in Sections 4.1 and 4.2, respectively. As mentioned in the Introduction, some first requirement for this to hold is that the effective heat capacity of the system is positive. This amounts to ask for

$$0 < \gamma_0 := \inf_{\theta>0}\left(c - \theta f''_*(\theta)\right) \tag{4.6}$$

which indeed follows with our actual choice of parameters, see Table 8.

4.1. Mechanical subproblem

Relation (4.4) can be rewritten as

$$R\partial|\boldsymbol{e}^{\mathrm{tr}}_i - \boldsymbol{e}^{\mathrm{tr}}_{i-1}| + (H + 2G)\boldsymbol{e}^{\mathrm{tr}}_i + f_*(\theta_i)\partial|\boldsymbol{e}^{\mathrm{tr}}_i|_\eta + \partial I(\boldsymbol{e}^{\mathrm{tr}}_i) \ni 2G\boldsymbol{e}_i. \tag{4.7}$$

For all given $\boldsymbol{e}^{\mathrm{tr}}_{i-1} \in \mathbb{R}^{3\times3}_{\mathrm{dev}}$, $\theta_i > 0$, and $\boldsymbol{e}_i := \boldsymbol{e}(t_i)$, relation (4.7) admits a unique solution $\boldsymbol{e}^{\mathrm{tr}}_i \in \mathbb{R}^{3\times3}_{\mathrm{dev}}$. Indeed, $\boldsymbol{e}^{\mathrm{tr}}_i$ is the unique minimizer of the uniformly convex functional

$$\boldsymbol{e}^{\mathrm{tr}} \mapsto R|\boldsymbol{e}^{\mathrm{tr}} - \boldsymbol{e}^{\mathrm{tr}}_{i-1}| + \frac{1}{2}(H + 2G)|\boldsymbol{e}^{\mathrm{tr}}|^2 + f_*(\theta_i)|\boldsymbol{e}^{\mathrm{tr}}|_\eta + I(\boldsymbol{e}^{\mathrm{tr}}) - 2G\boldsymbol{e}_i : \boldsymbol{e}^{\mathrm{tr}}.$$

Take now two different pairs of data $(\boldsymbol{e}^1_i, \theta^1_i)$ and $(\boldsymbol{e}^2_i, \theta^2_i)$ and let $\boldsymbol{e}^{\mathrm{tr},1}_i$ and $\boldsymbol{e}^{\mathrm{tr},2}_i$ be the corresponding solutions to (4.7). By taking the difference of the respective equations, testing on $\boldsymbol{e}^{\mathrm{tr},1}_i - \boldsymbol{e}^{\mathrm{tr},2}_i$, and exploiting monotonicity we obtain that

$$(H + 2G)|\boldsymbol{e}^{\mathrm{tr},1}_i - \boldsymbol{e}^{\mathrm{tr},2}_i|^2 \leq 2G(\boldsymbol{e}^1_i - \boldsymbol{e}^2_i) : (\boldsymbol{e}^{\mathrm{tr},1}_i - \boldsymbol{e}^{\mathrm{tr},2}_i) + (f_*(\theta_1) - f_*(\theta_2))\partial|\boldsymbol{e}^{\mathrm{tr},2}_i|_\eta : (\boldsymbol{e}^{\mathrm{tr},1}_i - \boldsymbol{e}^{\mathrm{tr},2}_i)$$

$$\leq \left(2G|\boldsymbol{e}^1_i - \boldsymbol{e}^2_i| + \beta|\theta_1 - \theta_2|\right)|\boldsymbol{e}^{\mathrm{tr},1}_i - \boldsymbol{e}^{\mathrm{tr},2}_i|.$$

Hence, we have checked the Lipschitz continuity

$$|e_i^{\mathrm{tr},1} - e_i^{\mathrm{tr},2}| \le \frac{2G}{H+2G}|e_i^1 - e_i^2| + \frac{\beta}{H+2G}|\theta_1 - \theta_2|. \tag{4.8}$$

Note that the well-posedness of (4.7) is indeed independent of the regularization η as well as of the truncation f_* and would hold also in absence of such modifications.

4.2. Thermal subproblem

Assume now to be given $\theta_{i-1} > 0$, $\theta_i^e := \theta^e(t_i) > 0$, and $e_i^{\mathrm{tr}} \in \mathbb{R}_{\mathrm{dev}}^{3\times3}$. Eq. (4.3) can be equivalently rewritten as

$$\gamma_\eta(y_{i-1})\theta_i - \frac{\tau_i\lambda}{\theta_i} = -\frac{\tau_i\lambda}{\theta_i^e} + \gamma_\eta(y_{i-1})\theta_{i-1} + R|e_i^{\mathrm{tr}} - e_{i-1}^{\mathrm{tr}}| + \theta_i f_*'(\theta_i)\partial|e_i^{\mathrm{tr}}|_\eta : (e_i^{\mathrm{tr}} - e_{i-1}^{\mathrm{tr}}). \tag{4.9}$$

As the map $\theta \in \mathbb{R}_+ \mapsto \gamma_\eta(y_{i-1})\theta - \lambda/\theta$ is injective and onto $\mathbb{R}$, for all $\tilde{\theta}$ we can find a unique solution $\theta_i > 0$ to the above equation where the term $\theta_i f_*'(\theta_i)$ on the right-hand side is replaced by $\tilde{\theta} f_*'(\tilde{\theta})$. This defines a map $\tilde{\theta} \mapsto \theta_i$ which can be proved to be a contraction under the condition

$$\phi_0 := \sup_\theta |f_*'(\theta) - \theta f_*''(\theta)| < \frac{\gamma_0}{2\epsilon_L}. \tag{4.10}$$

Indeed, assume to be given $\tilde{\theta}^1$ and $\tilde{\theta}^2$ and the corresponding solutions θ_i^1 and θ_i^2. Take the difference between equation (4.9) written for θ_i^1 and the same equation for θ_i^2 and test it on $\theta_i^1 - \theta_i^2$ in order to get that

$$\begin{aligned}\gamma_\eta(y_{i-1})|\theta_i^1 - \theta_i^2|^2 &\le |\tilde{\theta}^1 f_*'(\tilde{\theta}^1) - \tilde{\theta}^2 f_*'(\tilde{\theta}^2)|\,|e_i^{\mathrm{tr}} - e_{i-1}^{\mathrm{tr}}|\,|\theta_i^1 - \theta_i^2| \\ &\le 2\epsilon_L \sup_\theta\left(f_*'(\theta) - \theta f_*''(\theta)\right)|\tilde{\theta}^1 - \tilde{\theta}^2|\,|\theta_i^1 - \theta_i^2|.\end{aligned}$$

Also by using (4.6), we deduce the Lipschitz continuity bound

$$|\theta_i^1 - \theta_i^2| \le \frac{2\epsilon_L\phi_0}{\gamma_0}|\tilde{\theta}^1 - \tilde{\theta}^2| \tag{4.11}$$

for the map $\tilde{\theta} \mapsto \theta$. Under condition (4.10), this map is hence a contraction and relation (4.9) has a unique solution. We can directly check that indeed the solution θ_i is bounded from below, depending on data. To this aim, choose

$$\theta_{\min} = \min\{\theta_{i-1}, \theta_i^e, \theta_{\mathrm{tr}} - 2\rho\} > 0$$

and multiply (4.9) by $-(\theta_i - \theta_{\min})^- = \min\{\theta_i - \theta_{\min}, 0\} < 0$ getting

$$\begin{aligned}\gamma_\eta(y_{i-1})|(\theta_i - \theta_{\min})^-|^2 &= \gamma_\eta(y_{i-1})(\theta_{\min} - \theta_{i-1})(\theta_i - \theta_{\min})^- - \lambda\tau_i\left(\frac{1}{\theta_i} - \frac{1}{\theta_i^e}\right)(\theta_i - \theta_{\min})^- \\ &\quad - R|e_i^{\mathrm{tr}} - e_{i-1}^{\mathrm{tr}}|(\theta_i - \theta_{\min})^- - \theta_i f_*'(\theta_i)\partial|e_i^{\mathrm{tr}}|_\eta : (e_i^{\mathrm{tr}} - e_{i-1}^{\mathrm{tr}})(\theta_i - \theta_{\min})^-.\end{aligned} \tag{4.12}$$

The four terms on the above right-hand side are nonpositive. Indeed, the term $\gamma_\eta(y_{i-1})(\theta_{\min} - \theta_{i-1})(\theta_i - \theta_{\min})^-$ is nonpositive by (4.6) as $\theta_{\min} \le \theta_{i-1}$. Moreover, we have that

$$-\lambda\tau_i\left(\frac{1}{\theta_i} - \frac{1}{\theta_i^e}\right)(\theta_i - \theta_{\min})^- = -\lambda\tau_i\frac{\theta_i^e - \theta_i}{\theta_i\theta_i^e}(\theta_i - \theta_{\min})^- \le 0$$

as $0 < \theta_i \le \theta_{\min} \le \theta_i^e$ whenever $(\theta_i - \theta_{\min})^- \neq 0$. The nonpositivity of the term $-R|e_i^{\mathrm{tr}} - e_{i-1}^{\mathrm{tr}}|(\theta_i - \theta_{\min})^-$ is clear. As $f_*(\theta)$ vanishes for $\theta < \theta_{\mathrm{tr}} - 2\rho$ we finally have that

$$(\theta_i - \theta_{\min})^- \neq 0 \implies \theta_i f_*'(\theta_i)\partial|e_i^{\mathrm{tr}}|_\eta : (e_i^{\mathrm{tr}} - e_{i-1}^{\mathrm{tr}}) = 0.$$

Owing to the nonpositivity of the right-hand side of (4.12) and to (4.6) we have proved that $(\theta_i - \theta_{\min})^- = 0$ hence

$$\theta \ge \theta_{\min} > 0. \tag{4.13}$$

Let us now consider θ_i^1 and θ_i^2 to be the unique solutions of (4.9) with $\boldsymbol{e}_i^{\mathrm{tr}} = \boldsymbol{e}_i^{\mathrm{tr},1}$ and $\boldsymbol{e}_i^{\mathrm{tr}} = \boldsymbol{e}_i^{\mathrm{tr},2}$, respectively. By arguing as above we readily obtain that

$$\gamma_0 |\theta_i^1 - \theta_i^2|^2 \le R |\boldsymbol{e}_i^{\mathrm{tr},1} - \boldsymbol{e}_i^{\mathrm{tr},2}| \, |\theta_i^1 - \theta_i^2|$$
$$+ \left(\theta^1 f_*'(\theta^1) \partial |\boldsymbol{e}^{\mathrm{tr},1}|_\eta : (\boldsymbol{e}^{\mathrm{tr},1} - \boldsymbol{e}_{i-1}^{\mathrm{tr}}) - \theta^2 f_*'(\theta^2) \partial |\boldsymbol{e}^{\mathrm{tr},2}|_\eta : (\boldsymbol{e}^{\mathrm{tr},2} - \boldsymbol{e}_{i-1}^{\mathrm{tr}}) \right) (\theta_i^1 - \theta_i^2). \quad (4.14)$$

In the following, we will consider the case of temperature bounded from above by $\theta^* > 0$. By exploiting the Lipschitz continuity of $\partial |\cdot|_\eta$ and assuming $\theta_i^1, \theta_i^2 \le \theta^*$ one deduces that

$$\gamma_0 |\theta_i^1 - \theta_i^2| \le R |\boldsymbol{e}_i^{\mathrm{tr},1} - \boldsymbol{e}_i^{\mathrm{tr},2}| + 2\epsilon_L \phi_0 |\theta_i^1 - \theta_i^2| + \frac{2\epsilon_L \beta \theta_*}{\eta} |\boldsymbol{e}^{\mathrm{tr},1} - \boldsymbol{e}^{\mathrm{tr},2}| + \beta \theta_* |\boldsymbol{e}^{\mathrm{tr},1} - \boldsymbol{e}^{\mathrm{tr},2}|. \quad (4.15)$$

4.3. Existence for the discrete problem

Let us now check that the discrete system (4.3)–(4.4) can be solved for all given $\theta_{i-1} > 0$, $\boldsymbol{e}_{i-1}^{\mathrm{tr}} \in \mathbb{R}_{\mathrm{dev}}^{3\times3}$, $\theta_i^e > 0$, and $\boldsymbol{e}_i \in \mathbb{R}_{\mathrm{dev}}^{3\times3}$. The strategy here is to consider an iterative procedure, solving indeed the mechanical and the thermal problems sequentially.

For some trial

$$\tilde{\boldsymbol{e}}_i^{\mathrm{tr}} \in B := \{\boldsymbol{e}^{\mathrm{tr}} \in \mathbb{R}_{\mathrm{dev}}^{3\times3} \ : \ |\boldsymbol{e}^{\mathrm{tr}}| \le \epsilon_L\},$$

we find the unique solution $\tilde{\theta} = S^1(\tilde{\boldsymbol{e}}_i^{\mathrm{tr}})$ of (4.9) with $\boldsymbol{e}_i^{\mathrm{tr}} = \tilde{\boldsymbol{e}}_i^{\mathrm{tr}}$. Note that the map S^1 is Lipschitz continuous by (4.15). Then, we uniquely solve (4.7) with $\theta_i = \tilde{\theta}$ for $\boldsymbol{e}_i^{\mathrm{tr}} = S^2(\tilde{\theta})$. Recall from (4.8) that the solution operator S^2 is Lipschitz continuous as well. In conclusion, we have defined a Lipschitz continuous map $S = S^2 \circ S^1$ from the ball B to itself. Hence, S has a fixed point $\boldsymbol{e}^{\mathrm{tr}}$ by the classical Browder Theorem, and the pair $(\theta, \boldsymbol{e}^{\mathrm{tr}}) = (S^1(\boldsymbol{e}^{\mathrm{tr}}), \boldsymbol{e}^{\mathrm{tr}})$ solves (4.7) + (4.9).

Before closing this section let us remark that the above existence proof is nonconstructive. In particular, we are not in the position of proving that the iterative procedure actually converges, but rather that *some subsequence* of such iterations converges. Our numerical evidence shows however that this issue is not jeopardizing the performance of the algorithm. Namely, the numerical procedure always detects a fixed point.

4.4. Unconditional stability

In order to possibly check the unconditional stability of the scheme, as well as its convergence, let us introduce some assumptions on the data. In what follows we shall ask for

$$\theta^e \in W^{1,1}(0, T), \quad \theta^e \ge \theta_{\min}^e > 0, \quad \boldsymbol{e} \in W^{1,\infty}(0, T; \mathbb{R}_{\mathrm{dev}}^{3\times3}),$$
$$\theta_0 > 0, \quad \boldsymbol{e}_0^{\mathrm{tr}} \in B, \quad \exists \boldsymbol{e}_{-1}^{\mathrm{tr}} \in \mathbb{R}_{\mathrm{dev}}^{3\times3} \quad \text{such that}$$
$$R\partial |\boldsymbol{e}_0^{\mathrm{tr}} - \boldsymbol{e}_{-1}^{\mathrm{tr}}| + (H + 2G)\boldsymbol{e}_0^{\mathrm{tr}} + f(\theta_0)|\boldsymbol{e}_0^{\mathrm{tr}}|_\eta \ni 2G\boldsymbol{e}(0). \quad (4.16)$$

Moreover, let us introduce the short-hand notation for incremental quotients

$$\delta\theta_i = \frac{\theta_i - \theta_{i-1}}{\tau_i}, \quad \delta\boldsymbol{e}_i^{\mathrm{tr}} = \frac{\boldsymbol{e}_i^{\mathrm{tr}} - \boldsymbol{e}_{i-1}^{\mathrm{tr}}}{\tau_i},$$

and so on. In the following, the symbol C stands for any constant depending on data but not on the partition, and possibly varying from line to line.

By induction on i, the lower bound (4.13) entails the following uniform lower bound

$$\theta_i \ge \min\{\theta_0, \theta_{\min}^e, \theta_{\mathrm{tr}} - 2\rho\} =: \theta_{\min} > 0. \quad (4.17)$$

For the sake of later purposes, let us assume to have chosen θ_0, θ^e, and θ_{tr} in such a way that $\theta_{\min} > 250$ K.

We start by testing the temperature equation (4.9) by $\tau_i \delta\theta_i$ getting

$$\gamma_0 \tau_i |\delta\theta_i|^2 - \lambda(\log\theta_i - \log\theta_{i-1}) \le \frac{\lambda\tau_i}{\theta_i^e}\delta\theta_i + \tau_i R|\delta e_i^{\mathrm{tr}}|\delta\theta_i + \theta_i f_*'(\theta_i)\partial|e_i^{\mathrm{tr}}|_\eta : \delta e_i^{\mathrm{tr}}\delta\theta_i. \tag{4.18}$$

Let us now take the difference between (4.7) written at level i and the same relation at level $i = 1$. By making use of e_{-1}^{tr} from (4.16) this can be accomplished for all $i = 1, \ldots, m \le N$. We test this difference by δe_i^{tr} and exploit the fact that $\xi_i \in \partial R|e_i^{\mathrm{tr}} - e_{i-1}^{\mathrm{tr}}|$ iff $e_i^{\mathrm{tr}} - e_{i-1}^{\mathrm{tr}} \in \partial I_R(\xi_i)$ in order to deduce that

$$\tau_i(H + 2G)|\delta e_i^{\mathrm{tr}}|^2 \le \tau_i 2G\delta e_i : \delta e_i^{\mathrm{tr}} - \tau_i \delta f(\theta_i)\partial|e_i^{\mathrm{tr}}|_\eta : \delta e_i^{\mathrm{tr}}.$$

Let us now multiply the latter by $\theta_i > 0$ and add it to (4.18) getting

$$\gamma_0\tau_i|\delta\theta_i|^2 - \lambda(\log\theta_i - \log\theta_{i-1}) + \tau_i\theta_i(H + 2G)|\delta e_i^{\mathrm{tr}}|^2$$

$$\le \frac{\lambda\tau_i}{\theta_i^e}\delta\theta_i + \tau_i R|\delta e_i^{\mathrm{tr}}|\delta\theta_i + \tau_i\theta_i(f_*'(\theta_i)\delta\theta_i - \delta f(\theta_i))\partial|e_i^{\mathrm{tr}}|_\eta : \delta e_i^{\mathrm{tr}} + \tau_i 2G\theta_i\delta e_i : \delta e_i^{\mathrm{tr}}$$

$$= \frac{\lambda\tau_i}{\theta_i^e}\delta\theta_i + \tau_i R|\delta e_i^{\mathrm{tr}}|\delta\theta_i + \tau_i^2\theta_i\frac{f_*''(\tilde\theta)}{2}|\partial\theta_i|^2\partial|e_i^{\mathrm{tr}}|_\eta : \delta e_i^{\mathrm{tr}} + \tau_i 2G\theta_i\delta e_i : \delta e_i^{\mathrm{tr}}$$

$$\le \tau_i C|\delta\theta_i| + \tau_i R|\delta e_i^{\mathrm{tr}}|\,|\delta\theta_i| + \tau_i\frac{\epsilon_L\beta\theta_*}{2\rho}|\delta\theta_i|^2 + \tau_i C|\theta_i|\,|\delta e_i^{\mathrm{tr}}|$$

where $\tilde\theta$ is an intermediate value between θ_i and θ_{i-1}. By taking the sum of the latter inequality for $i = 1, \ldots, m \le N$ we deduce

$$\left(\gamma_0 - \frac{\epsilon_L\beta\theta_*}{2\rho}\right)\sum_{i-1}^m \tau_i|\delta\theta_i|^2 - \lambda\log\theta_m + \sum\tau_i\theta_i(H + 2G)|\delta e_i^{\mathrm{tr}}|^2$$

$$\le C + C\sum_{i-1}^m \tau_i|\delta\theta_i| + R\sum_{i-1}^m \tau_i|\delta e_i^{\mathrm{tr}}|\,|\delta\theta_i| + C\sum_{i-1}^m \tau_i|\theta_i|\,|\delta e_i^{\mathrm{tr}}|. \tag{4.19}$$

Under the compatibility conditions

$$\gamma_0 - \frac{\epsilon_L\beta\theta_*}{2\rho} > 0 \quad\text{and}\quad R^2 < \theta_{\min}\gamma_0(H + 2G), \tag{4.20}$$

which are satisfied by our data set (see Table 8) by letting, for instance, $\theta_* = 450$ K and $\rho = 30$ K and recalling that $\theta_{\min} > 250$ K, one has that

$$\sum_{i=1}^N \tau_i(|\delta\theta_i|^2 + |\delta e_i^{\mathrm{tr}}|^2) \le C. \tag{4.21}$$

4.5. Convergence

Let us consider a sequence of partitions $\{t_i\}$ so that the corresponding maximal time step $\tau = \max_i(t_i - t_{i-1})$ converges to 0. We shall index these partitions by their diameter τ. Letting $\{u_i\}_{i=0}^N$ be a vector, we denote by $u_\tau, \overline{u}_\tau, \underline{u}_\tau$ three functions of the time interval $[0, T]$ which interpolate the values of the generic vector $\{u_i\}$ on the partition with size τ. In particular, for all $t \in (t_{i-1}, t_i], i = 1, \ldots, N$,

$$u_\tau(0) := u_0, \qquad u_\tau(t) := \alpha_i(t)u_i + (1 - \alpha_i(t))u_{i-1},$$
$$\overline{u}_\tau(0) := u_0, \qquad \overline{u}_\tau(t) := u_i,$$
$$\underline{u}_\tau(0) := u_0, \qquad \underline{u}_\tau(t) = u_{i-1}$$

where

$$\alpha_i(t) := (t - t_{i-1})/\tau_i.$$

Owing to these notations we can rewrite the discrete system (4.3)–(4.4) in the compact form

$$\gamma_\eta(\underline{\mathbf{y}}_\tau)\dot{\theta}_\tau - \frac{\lambda}{\overline{\theta}_\tau} = -\frac{\lambda}{\overline{\theta}_\tau^e} + R|\dot{\mathbf{e}}_\tau^{\mathrm{tr}}| + \overline{\theta}_\tau f_*'(\overline{\theta}_\tau)\partial|\overline{\mathbf{e}}_\tau^{\mathrm{tr}}|_\eta : \dot{\mathbf{e}}_\tau^{\mathrm{tr}}, \tag{4.22}$$

$$\overline{\boldsymbol{\eta}}_\tau + (H + 2G)\overline{\mathbf{e}}_\tau^{\mathrm{tr}} + f_*(\overline{\theta}_\tau)\partial|\overline{\mathbf{e}}_\tau^{\mathrm{tr}}|_\eta + \overline{\boldsymbol{\xi}}_\tau = 2G\overline{\mathbf{e}}_\tau, \tag{4.23}$$

$$\overline{\boldsymbol{\eta}}_\tau \in R\partial|\dot{\mathbf{e}}_\tau^{\mathrm{tr}}|, \qquad \overline{\boldsymbol{\xi}}_\tau \in \partial I(\overline{\mathbf{e}}_\tau^{\mathrm{tr}}) \tag{4.24}$$

for almost all $t \in (0, T)$. In particular, by the boundedness of $\partial|\cdot|$ and $\partial|\cdot|_\eta$ one obtains from the bound (4.21) and by comparison in (4.23) that the norms

$$\|\theta_\tau\|_{H^1}, \ \|\mathbf{e}_\tau^{\mathrm{tr}}\|_{H^1}, \ \|\overline{\boldsymbol{\eta}}_\tau\|_{L^\infty}, \ \|\overline{\boldsymbol{\xi}}_\tau\|_{L^\infty} \text{ are bounded, independently of } \tau.$$

Hence, we can extract not relabeled subsequences such that

$$\theta_\tau \to \theta \quad \text{strongly in } C[0, T] \text{ and weakly in } H^1(0, T), \tag{4.25}$$

$$\overline{\theta}_\tau, \ \underline{\theta}_\tau \to \theta \quad \text{strongly in } L^\infty(0, T), \tag{4.26}$$

$$\mathbf{e}_\tau^{\mathrm{tr}} \to \mathbf{e}^{\mathrm{tr}} \quad \text{strongly in } C([0, T]; \mathbb{R}_{\mathrm{dev}}^{3\times3}) \text{ and weakly in } H^1(0, T; \mathbb{R}_{\mathrm{dev}}^{3\times3}), \tag{4.27}$$

$$\overline{\mathbf{e}}_\tau^{\mathrm{tr}}, \ \underline{\mathbf{e}}_\tau^{\mathrm{tr}} \to \mathbf{e}^{\mathrm{tr}} \quad \text{strongly in } L^\infty(0, T; \mathbb{R}_{\mathrm{dev}}^{3\times3}), \tag{4.28}$$

$$\overline{\boldsymbol{\eta}}_\tau \to \boldsymbol{\eta} \quad \text{weakly star in } L^\infty(0, T; \mathbb{R}_{\mathrm{dev}}^{3\times3}), \tag{4.29}$$

$$\overline{\boldsymbol{\xi}}_\tau \to \boldsymbol{\xi} \quad \text{weakly star in } L^\infty(0, T; \mathbb{R}_{\mathrm{dev}}^{3\times3}), \tag{4.30}$$

We shall now pass to the limit in relations (4.22)–(4.24). By using also the uniform positivity of $\underline{\theta}_\tau$ from (4.17) we have that $\gamma_\eta(\underline{\mathbf{y}}_\tau) \to \gamma_\eta(\mathbf{y})$ strongly in $L^\infty(0, T)$ so that convergence (4.25) entails that $\gamma_\eta(\underline{\mathbf{y}}_\tau)\dot{\theta}_\tau \to \gamma_\eta(\mathbf{y})\dot{\theta}$ weakly in $L^2(0, T)$. The convergence of the terms $-\lambda/\overline{\theta}_\tau \to -\lambda/\theta$ and $-\lambda/\overline{\theta}_\tau^e \to -\lambda/\theta^e$ in $L^\infty(0, T)$ follows by the strict bound (4.17), convergence (4.26), and the fact that $\overline{\theta}_\tau^e \to \theta^e$ in $C[0, T]$. Moreover, we readily check that

$$\overline{\theta}_\tau f_*'(\overline{\theta}_\tau)\partial|\overline{\mathbf{e}}_\tau^{\mathrm{tr}}|_\eta : \dot{\mathbf{e}}_\tau^{\mathrm{tr}} \to \theta f_*'(\theta)\partial|\mathbf{e}^{\mathrm{tr}}|_\eta : \dot{\mathbf{e}}^{\mathrm{tr}} \quad \text{weakly in } L^2(0, T; \mathbb{R}_{\mathrm{dev}}^{3\times3})$$

where we have in particular used the Lipschitz continuity of $\partial|\cdot|_\eta$. We can pass to the limit in each term in (4.23) getting

$$\boldsymbol{\eta} + (H + 2G)\mathbf{e}^{\mathrm{tr}} + f_*(\theta)\partial|\mathbf{e}^{\mathrm{tr}}|_\eta + \boldsymbol{\xi} = 2G\mathbf{e}. \tag{4.31}$$

In addition, by the classical strong–weak closure of subdifferentials we get that $\boldsymbol{\xi} \in \partial I(\mathbf{e}^{\mathrm{tr}})$ almost everywhere in time. In order to identify $\boldsymbol{\eta}$ we proceed by lower semicontinuity by computing

$$\limsup_{\tau\to0}\left(\int_0^T \overline{\boldsymbol{\eta}}_\tau : \dot{\mathbf{e}}_\tau^{\mathrm{tr}}\,\mathrm{d}t\right) \le \limsup_{\tau\to0}\left(-\frac{H+2G}{2}(|\mathbf{e}_\tau^{\mathrm{tr}}(T)|^2 - |\mathbf{e}_0^{\mathrm{tr}}|^2) - I(\mathbf{e}_\tau^{\mathrm{tr}}(T)) + I(\mathbf{e}_0^{\mathrm{tr}})\right.$$

$$\left. -\int_0^T f_*(\overline{\theta}_\tau)\partial|\overline{\mathbf{e}}_\tau^{\mathrm{tr}}|_\eta : \dot{\mathbf{e}}_\tau^{\mathrm{tr}}\,\mathrm{d}t + \int_0^T 2G\overline{\mathbf{e}}_\tau : \dot{\mathbf{e}}_\tau^{\mathrm{tr}}\,\mathrm{d}t\right)$$

$$\le -\frac{H+2G}{2}(|\mathbf{e}^{\mathrm{tr}}(T)|^2 - |\mathbf{e}_0^{\mathrm{tr}}|^2) - I(\mathbf{e}^{\mathrm{tr}}(T)) + I(\mathbf{e}_0^{\mathrm{tr}}) - \int_0^T f_*(\theta)\partial|\mathbf{e}^{\mathrm{tr}}|_\eta : \dot{\mathbf{e}}^{\mathrm{tr}}\,\mathrm{d}t$$

$$- \int_0^T 2G\mathbf{e} : \dot{\mathbf{e}}^{\mathrm{tr}}\,\mathrm{d}t = \int_0^T \boldsymbol{\eta} : \dot{\mathbf{e}}^{\mathrm{tr}}\,\mathrm{d}t.$$

In particular, by the classical result [58, Prop. 2.5, p. 27] we obtain that $\boldsymbol{\eta} \in R\partial|\dot{\mathbf{e}}^{\mathrm{tr}}|$ almost everywhere and

$$\int_0^T R|\dot{\mathbf{e}}_\tau^{\mathrm{tr}}|\,\mathrm{d}t = \int_0^T \overline{\boldsymbol{\eta}}_\tau : \dot{\mathbf{e}}_\tau^{\mathrm{tr}}\,\mathrm{d}t \to \int_0^T \boldsymbol{\eta} : \dot{\mathbf{e}}^{\mathrm{tr}}\,\mathrm{d}t = \int_0^T R|\dot{\mathbf{e}}^{\mathrm{tr}}|\,\mathrm{d}t.$$

The above estimate can be also localized to subsets $[s, t] \subset [0, T]$ so that it indeed entails the convergence $R|\dot{\mathbf{e}}_\tau^{\mathrm{tr}}| \to R|\dot{\mathbf{e}}^{\mathrm{tr}}|$ in $L^1(0, T)$. This concludes the convergence proof.

5. Numerical results

The aim of this section is to illustrate the performance of the proposed semi-implicit scheme. We shall implement the discretization procedure described in Section 4.3. Given a time partition $\{t_i\}$, initial data $(\theta_0, e_0^{\mathrm{tr}})$, and possibly time-dependent external data $i \mapsto (\theta_i^e, e_i)$, we solve the system (4.3)–(4.4) for $i = 1, \ldots, N$ by iterating, at each time step, the solution of the mechanical and thermal subproblems until convergence. As the computationally observed temperatures do not exceed the threshold $\theta_* - 2\rho$, no actual truncation of f is needed in the algorithm. We shall hence keep the notation f in the remainder of the section.

From the algorithmical viewpoint, the solution of the iteration in the (scalar) thermal subproblem is straightforward. On the other hand, the discussion of the mechanical subproblem, namely relation (4.7), is more delicate so that we shall concentrate on the latter. Indeed, the interplay of the three nonlinear terms of relation (4.7) is at the same time a distinctive feature of the model and a criticality, in term of the use of generalized Newton methods. The introduced regularization $|\cdot|_\eta$ of a norm in (4.7) is clearly beneficial from the algorithmical viewpoint. This approximation is widely used in this context [17–19,49] and has been proved to converge to the nonregularized situation for $\eta \to 0$ in a number of relevant cases [50]. Still, this regularization is to a large extent not needed here, as we comment in the following subsection.

5.1. Nonregularized case in (4.7)

We shall collect here some discussion on the possibility of considering directly the nonregularized case $\eta = 0$ in relation (4.7). Although not accessible to a complete theoretical analysis, the nonregularized case corresponds to the original formulation of the material relation. As such, we believe it to be of interest from both the modeling and numerical viewpoint.

Given data $\theta_i > 0$ and e_{i-1}^{tr}, $e_i \in \mathbb{R}_{\mathrm{dev}}^{3\times3}$, the idea is to perform some *a priori* tests in order to check if the solution e_i^{tr} of relation (4.7) is

neither $\{e_{i-1}^{\mathrm{tr}}\}$ nor $\{\mathbf{0}\}$,

which exactly correspond to the singular sets of the nonlinearities $\partial|e^{\mathrm{tr}} - e_{i-1}^{\mathrm{tr}}|$ and $\partial|e^{\mathrm{tr}}|$ (that is $\partial|e^{\mathrm{tr}}|_\eta$ for $\eta = 0$) in (4.7), respectively (the treatment of the constraint $\partial I(e_i^{\mathrm{tr}})$ follows *ex post*, see below). We shall proceed by distinguishing mutual cases.

Case (1): $e_i^{\mathrm{tr}} = e_{i-1}^{\mathrm{tr}} = \mathbf{0}$. In this case relation (4.7) corresponds to

$$(R + f(\theta_i))B \ni 2Ge_i$$

where $B = \{|e^{\mathrm{tr}}| \leq 1\}$ is the unit ball. This can be achieved iff

$$2G|e_i| \leq R + f(\theta_i). \tag{5.1}$$

Case (2): $e_{i-1}^{\mathrm{tr}} \neq e_i^{\mathrm{tr}} = \mathbf{0}$. Here, relation (4.7) reads

$$R\frac{e_{i-1}^{\mathrm{tr}}}{|e_{i-1}^{\mathrm{tr}}|} + f(\theta_i)B \ni 2Ge_i$$

which can be fulfilled iff

$$\left| 2Ge_i - R\frac{e_{i-1}^{\mathrm{tr}}}{|e_{i-1}^{\mathrm{tr}}|} \right| \leq f(\theta_i). \tag{5.2}$$

Case (3): $e_i^{\mathrm{tr}} = e_{i-1}^{\mathrm{tr}} \neq \mathbf{0}$ and $|e_i^{\mathrm{tr}}| < \epsilon_L$. We can rewrite relation (4.7) as

$$RB + (H + 2G)\frac{e_{i-1}^{\mathrm{tr}}}{|e_{i-1}^{\mathrm{tr}}|} + f(\theta_i)\frac{e_{i-1}^{\mathrm{tr}}}{|e_{i-1}^{\mathrm{tr}}|} \ni 2Ge_i$$

which holds iff

$$\left| 2Ge_i - (H + 2G)e_{i-1}^{\text{tr}} - f(\theta_i)\frac{e_{i-1}^{\text{tr}}}{|e_{i-1}^{\text{tr}}|} \right| \leq R. \tag{5.3}$$

Case (4): $e_i^{\text{tr}} = e_{i-1}^{\text{tr}}$ and $|e_i^{\text{tr}}| = \epsilon_L$. In this situation relation (4.7) reads

$$RB + (H + 2G)\frac{e_{i-1}^{\text{tr}}}{|e_{i-1}^{\text{tr}}|} + f(\theta_i)\frac{e_{i-1}^{\text{tr}}}{|e_{i-1}^{\text{tr}}|} + \ell\frac{e_{i-1}^{\text{tr}}}{|e_{i-1}^{\text{tr}}|} \ni 2Ge_i$$

where $\ell \geq 0$ is the (norm of the) Lagrange multiplier corresponding to the constraint $|e_i^{\text{tr}}| \leq \epsilon_L$. The inclusion holds iff, by letting

$$\boldsymbol{d} := \frac{e_{i-1}^{\text{tr}}}{|e_{i-1}^{\text{tr}}|}, \qquad \boldsymbol{w} := 2Ge_i - (H + 2G)e_{i-1}^{\text{tr}} - f(\theta_i)\frac{e_{i-1}^{\text{tr}}}{|e_{i-1}^{\text{tr}}|},$$

one has that

$$\boldsymbol{w} \in [0, \infty)\boldsymbol{d} + RB.$$

This is equivalent to ask for $\ell \geq 0$ and $|\boldsymbol{x}| \leq R$ such that $\boldsymbol{w} = \ell\boldsymbol{d} + \boldsymbol{x}$. Given $\boldsymbol{w}$ and $\boldsymbol{d}$, this condition can be readily checked to hold iff

$$(\boldsymbol{w} : \boldsymbol{d} \leq 0 \text{ and } |\boldsymbol{w}| \leq R) \quad \text{or} \quad (\boldsymbol{w} : \boldsymbol{d} > 0 \text{ and } |\boldsymbol{w} - (\boldsymbol{w} : \boldsymbol{d})\boldsymbol{d}| \leq R). \tag{5.4}$$

By performing the checks (5.1)–(5.4) we can identify the singular situations $e_i^{\text{tr}} = e_{i-1}^{\text{tr}}$ or $e_i^{\text{tr}} = \boldsymbol{0}$ completely. In case $e_i^{\text{tr}} \neq e_{i-1}^{\text{tr}}$ and $e_i^{\text{tr}} \neq \boldsymbol{0}$, we may proceed in solving relation

$$R\partial|e_i^{\text{tr}} - e_{i-1}^{\text{tr}}| + (H + 2G)e_i^{\text{tr}} + f(\theta_i)\partial|e_i^{\text{tr}}| \ni 2Ge_i, \tag{5.5}$$

which is nothing but (4.7) where the constraint $\partial I(e_i^{\text{tr}})$ has been removed. Relation (5.5) also admits a unique solution $\tilde{e}_i^{\text{tr}}$, which we have already checked to be different from e_{i-1}^{tr} and $\boldsymbol{0}$. In particular, we can avoid regularizing the norms in (5.5) as long as we remain in a neighborhood of the solution $\tilde{e}_i^{\text{tr}}$.

Eventually, if $|\tilde{e}_i^{\text{tr}}| \leq \epsilon_L$ then $e_i^{\text{tr}} = \tilde{e}_i^{\text{tr}}$ is the unique solution of (4.7). On the contrary, one has to treat directly (4.7), where now $\eta = 0$ is allowed. On the other hand, the constraining term $\partial I(e_i^{\text{tr}})$ could be regularized by penalization as

$$\partial I_\zeta(e_i^{\text{tr}}) = \frac{1}{\zeta}((|e_i^{\text{tr}}| - \epsilon_L)^+)^2\frac{e_i^{\text{tr}}}{|e_i^{\text{tr}}|}$$

where $\zeta > 0$ is a user-defined parameter. For all positive ζ the regularized term is Lipschitz continuous and it can be checked that the ζ-regularized solution to (4.7) converges as $\zeta \to 0$ to the solution of the nonregularized equation [50].

5.2. Implementation

The strain- and external-temperature-driven constitutive-model driver has been implemented in the *Mathematica* (*Wolfram*) environment and has been tested under different conditions.

The algorithm solves the time-discrete scheme from Section 4, along with the provisions of Section 5.1. At each time t_i, the values $e_i \in \mathbb{R}^{3\times3}_{\text{dev}}$, $\theta_i^e > 0$ are given as well as the previous states $\theta_{i-1} > 0$ and $e_{i-1}^{\text{tr}} \in \mathbb{R}^{3\times3}_{\text{dev}}$. The algorithm computes the actual values $\theta_i > 0$ and $e_i^{\text{tr}} \in \mathbb{R}^{3\times3}_{\text{dev}}$. The procedure is iterative and it is summarized in Table 1 and in the related sub-cycles.

In particular, the thermal subproblem is also solved iteratively. At each step one solves a scalar nonlinear equation. This iteration is actually a contraction, so that geometric convergence can be guaranteed.

On the contrary, the mechanical subproblem is solved directly. Firstly, one analyzes the four cases presented in Section 5.1. If all the corresponding checks fail, the solution of the mechanical subproblem is obtained by directly solving the nonlinear system. The (failure of the) preliminary checks ensure that the equation is smooth at the solution. In particular, a Newton–Raphson solution procedure, possibly in combination with a constraint, can be used.

Table 1

Implementation algorithm for the strain- and external-temperature-driven driver (see Tables 2 and 3).

Main algorithm

Starting data: $\{\boldsymbol{e}_i, \theta_i^{\mathrm{e}}\} \in \mathbb{R}^{3\times3}_{\mathrm{dev}} \times \mathbb{R}_+$ and $\{\boldsymbol{e}^{\mathrm{tr}}_{i-1}, \theta_{i-1}\} \in \mathbb{R}^{3\times3}_{\mathrm{dev}} \times \mathbb{R}_+$

Define $\boldsymbol{e}^{\mathrm{tr}}_{i,0} = \boldsymbol{e}^{\mathrm{tr}}_{i-1}$.

while $k \geq 1$, $|\theta_{i,k}-\theta_{i,k-1}|/\theta_{i,k} \geq tol$, *and* $|\boldsymbol{e}^{\mathrm{tr}}_{i,k}-\boldsymbol{e}^{\mathrm{tr}}_{i,k-1}|/|\boldsymbol{e}^{\mathrm{tr}}_{i,k}| \geq tol$ **do**

    Solve the **thermal subproblem** from Subsection 4.2:
    given $\{\theta_i^{\mathrm{e}}, \theta_{i-1}, \boldsymbol{e}^{\mathrm{tr}}_{i-1}\} \in \mathbb{R}_+ \times \mathbb{R}_+ \times \mathbb{R}^{3\times3}_{\mathrm{dev}}$ and $\boldsymbol{e}^{\mathrm{tr}}_{i,k-1} \in \mathbb{R}^{3\times3}_{\mathrm{dev}}$
    find $\theta_{i,k} > 0$ solving (4.9)
    (see Table 2).

    Solve the **mechanical subproblem** from Subsection 4.1:
    given $\{\boldsymbol{e}_i, \theta_{i,k}\} \in \mathbb{R}^{3\times3}_{\mathrm{dev}} \times \mathbb{R}_+$ and $\boldsymbol{e}^{\mathrm{tr}}_{i-1} \in \mathbb{R}^{3\times3}_{\mathrm{dev}}$
    find $\boldsymbol{e}^{\mathrm{tr}}_{i,k} \in \mathbb{R}^{3\times3}_{\mathrm{dev}}$ solving (5.5)
    (see Table 3).

end

Table 2

Algorithm for the thermal subproblem.

Thermal subproblem

Starting data: $\{\boldsymbol{e}_i, \theta_i^{\mathrm{e}}\} \in \mathbb{R}^{3\times3}_{\mathrm{dev}} \times \mathbb{R}_+$, $\boldsymbol{e}^{\mathrm{tr}}_{i-1}$, $\boldsymbol{e}^{\mathrm{tr}}_i \in \mathbb{R}^{3\times3}_{\mathrm{dev}}\theta_{i-1} > 0$

Define $\theta_{i,0} = \theta_{i-1}$.

while $k \geq 1$ *and* $|\theta_{i,k}-\theta_{i,k-1}|/\theta_{i,k} \geq tol$ **do**

    Find $\theta_{i,k} > 0$ solving

$$\gamma_\eta(\boldsymbol{y}_{i-1})\theta_i - \frac{\tau_i\lambda}{\theta_i} = -\frac{\tau_i\lambda}{\theta_i^{\mathrm{e}}} + \gamma_\eta(\boldsymbol{y}_{i-1})\theta_{i-1}$$
$$+ R|\boldsymbol{e}^{\mathrm{tr}}_i - \boldsymbol{e}^{\mathrm{tr}}_{i-1}| + \theta_{i,k-1}f'_*(\theta_{i,k-1})\partial|\boldsymbol{e}^{\mathrm{tr}}_i|_\eta : (\boldsymbol{e}^{\mathrm{tr}}_i - \boldsymbol{e}^{\mathrm{tr}}_{i-1}).$$

end

Table 3

Algorithm for the mechanical subproblem (see Tables 4–7).

Mechanical subproblem

Starting data: $\{\boldsymbol{e}_i, \theta_i\} \in \mathbb{R}^{3\times3}_{\mathrm{dev}} \times \mathbb{R}_+$, and $\boldsymbol{e}^{\mathrm{tr}}_{i-1} \in \mathbb{R}^{3\times3}_{\mathrm{dev}}$.

Check Cases (1) to (4), see Tables 4-7.

if Checks (1) to (4) fail **then**
    find $\tilde{\boldsymbol{e}}^{\mathrm{tr}}_i \in \mathbb{R}^{3\times3}_{\mathrm{dev}}$ solving
$$R\partial|\tilde{\boldsymbol{e}}^{\mathrm{tr}}_i - \boldsymbol{e}^{\mathrm{tr}}_{i-1}| + (H+2G)\tilde{\boldsymbol{e}}^{\mathrm{tr}}_i + f(\theta_i)\partial|\tilde{\boldsymbol{e}}^{\mathrm{tr}}_i| \ni 2G\boldsymbol{e}_i$$
    by Newton-Raphson.
end
if $|\tilde{\boldsymbol{e}}^{\mathrm{tr}}_i| \leq \varepsilon_L$ **then**
    define $\boldsymbol{e}^{\mathrm{tr}}_i = \tilde{\boldsymbol{e}}^{\mathrm{tr}}_i$.
end
if $|\tilde{\boldsymbol{e}}^{\mathrm{tr}}_i| > \varepsilon_L$ **then**
    define $\boldsymbol{e}^{\mathrm{tr}}_i$ by solving the system
$$R\partial|\boldsymbol{e}^{\mathrm{tr}}_i - \boldsymbol{e}^{\mathrm{tr}}_{i-1}| + (H+2G)\boldsymbol{e}^{\mathrm{tr}}_i + f(\theta_i)\partial|\boldsymbol{e}^{\mathrm{tr}}_i| \ni 2G\boldsymbol{e}_i \quad \text{and} \quad |\boldsymbol{e}^{\mathrm{tr}}_i| = \varepsilon_L$$
    by Newton-Raphson.
end

Table 4
Test for Case (1).

Check Case (1)
if $2G\|e_i\| \leq R + f(\theta_i)$ **then** $\quad e_i^{tr} = e_{i-1}^{tr}$ **end**

Table 5
Test for Case (2).

Check Case (2)
if $\left\| 2Ge_i + R\dfrac{e_{i-1}^{tr}}{\|e_{i-1}^{tr}\|} \right\| \leq f(\theta_i)$ **then** $\quad e_i^{tr} = 0$ **end**

Table 6
Test for Case (3).

Check Case (3)
if $\left\| 2Ge_i - (H + 2G)e_{i-1}^{tr} - f(\theta_i)\dfrac{e_{i-1}^{tr}}{\|e_{i-1}^{tr}\|} \right\| \leq R$ **then** $\quad e_i^{tr} = e_{i-1}^{tr}$ **end**

Table 7
Test for Case (4).

Check Case (4)
Define $\boldsymbol{d} := e_{i-1}^{tr}/\|e_{i-1}^{tr}\|$, $\boldsymbol{w} := 2Ge_i - (H+2G)e_{i-1}^{tr} - f(\theta_i)e_{i-1}^{tr}/\|e_{i-1}^{tr}\|$.   **if** $\boldsymbol{w}{:}\boldsymbol{d} \leq 0$ and $\|\boldsymbol{w}\| \leq R$ **then** $\quad e_i^{tr} = e_{i-1}^{tr}$ **end**   **if** $\boldsymbol{w}{:}\boldsymbol{d} > 0$ and $\|\boldsymbol{w}-(\boldsymbol{w}{:}\boldsymbol{d})\boldsymbol{d}\| \leq R$ **then** $\quad e_i^{tr} = e_{i-1}^{tr}$ **end**

5.3. Material parameters

The parameters used in the simulations are taken from [59] and are listed in Table 8. It can be verified that the adopted parameters satisfy conditions (4.6) and (4.20).

5.4. Proportional tests

In the following, numerical results corresponding to different proportional tests are displayed. The imposed proportional strain is of the form

$$
t \mapsto \boldsymbol{\varepsilon}(t) = \boldsymbol{e}(t) = \varepsilon_V(t) \begin{bmatrix} \sqrt{\dfrac{2}{3}} & 0 & 0 \\ 0 & -\dfrac{1}{\sqrt{6}} & 0 \\ 0 & 0 & -\dfrac{1}{\sqrt{6}} \end{bmatrix}
$$

where the time-dependent function $t \mapsto \varepsilon_V(t) \in \mathbb{R}$ is given.

Table 8
Material and numerical parameters.

Symbol	Value	Unit	Description
E	45 000	MPa	Young's modulus
ν	0.3	–	Poisson's coefficient
K	37 500	MPa	Bulk modulus
G	17 308	MPa	Shear modulus
R	110	MPa	Critical stress
β	4.49	MPa/K	Coefficient of function f
H	1000	MPa	Hardening constant
θ_{tr}	343	K	Martensite finish temperature
ϵ_L	0.049	–	Saturation strain limit
θ_0	300	K	Initial temperature
θ^e	390	K	External temperature
c	3.22	MPa/K	Specific heat
λ	2×10^3	(MPa K)/s	Heat exchange coefficient
ρ	31	K	Parameter in the definition of f
tol	10^{-6}	–	Tolerance
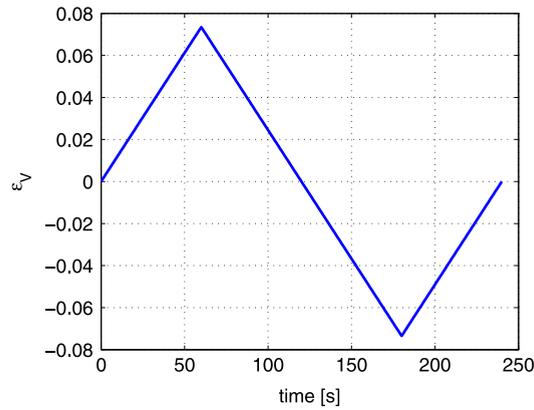
Fig. 1. First strain history: trend of the variable ε_V.

A first choice for ε_V is illustrated in Fig. 1. A single tension–compression cycle is performed. In order to clarify the material mechanisms, the first simulation is performed in pure martensitic conditions, with $\theta^e = \theta^0 = 300$ K, and the second one is performed in purely superelastic conditions, with $\theta^e = \theta^0 = 380$ K.

The response of the first test is reported in Fig. 2. Under the temperature transformation region, the only possible transformations regard the martensite reorientation: such mechanism provides a heat release, as it is clearly visible in the right plot of Fig. 2. Indeed, the temperature of the material increases during the martensite detwinning, despite the heat absorption by the external environment. In the elastic regions, the temperature change is only due to the exchange with the external environment.

The response of the second test is reported in Fig. 3. As before, we have heat release during the forward austenite-to-martensite transformation. In this case, since the material is in the superelastic region, heat absorption occurs during reverse martensite-to-austenite transformation. Again, in the elastic region the temperature only depends on the heat exchange with the external environment.

The third proportional test is performed using the parameters in Table 8. The corresponding mechanical and thermal response curves are displayed in Fig. 4. It can be clearly noted that the forward transformation produces a temperature increase, which in turn pulls the strain–stress curve towards higher-stress-level zones. Until time 70, the material stays under the transformation temperature. Therefore, the temperature can only increase, because of both the forward phase transformation, and the heat exchange with the external environment (indeed, the external temperature is here fixed to be $\theta^e = 390$ K). Below the transformation temperature, only martensitic reorientation takes place and releases heat.
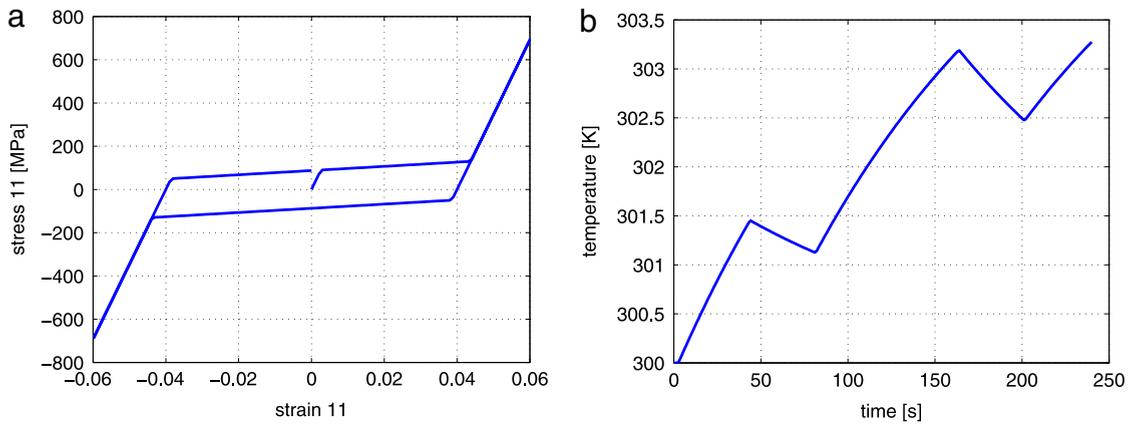
Fig. 2. First strain history, martensitic conditions case: strain 11 versus stress 11 plot (a) and temperature plot (b).
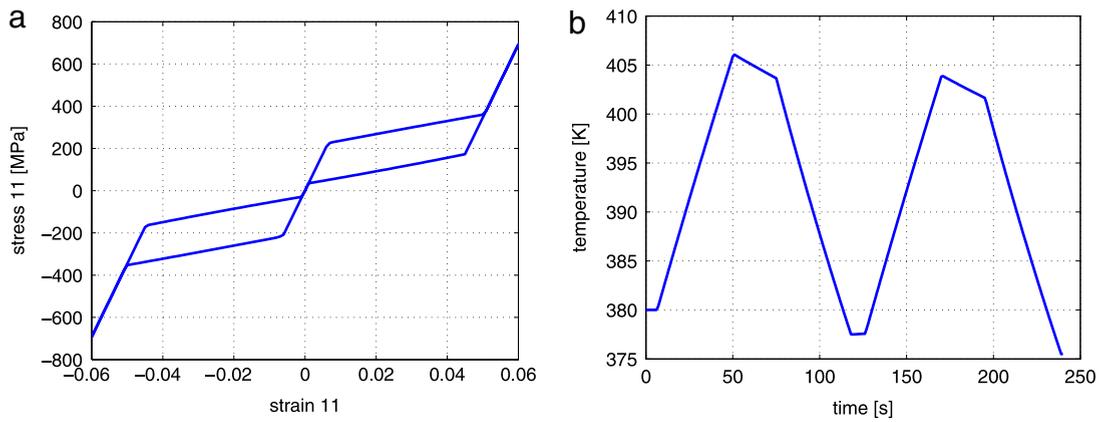

Fig. 3. First strain history, superelastic conditions case: strain 11 versus stress 11 plot (a) and temperature plot (b).
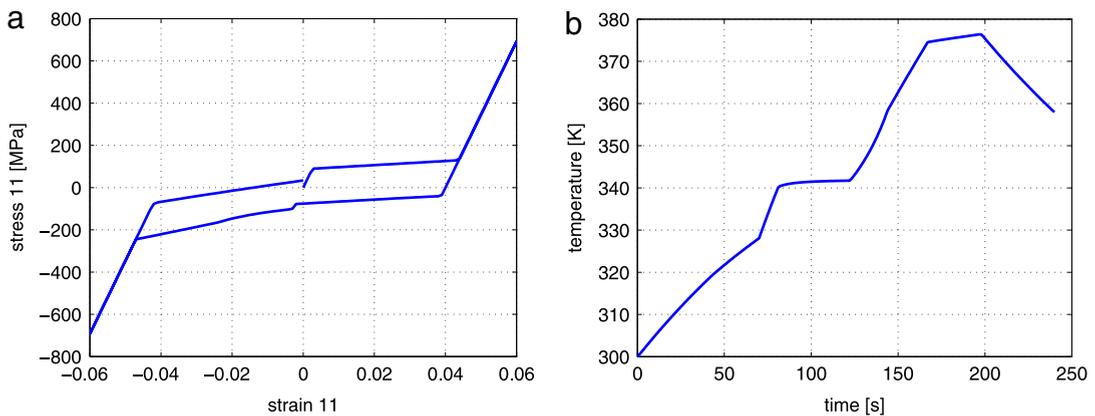

Fig. 4. First strain history, with initial and external temperatures defined in Table 8: strain 11 versus stress 11 plot (a) and temperature plot (b).

At time 70, the material enters the transition zone, individuated by $[\theta - \rho; \theta + \rho]$, so that during the forward transformation the heat release is even higher than the heat amount released at lower temperatures. At time 81, the reverse transformation takes place, absorbing heat. From time 123, a new forward transformation generated by compression occurs, so that we have heat release again. At time 125, the transformation temperature (i.e. the center of the transformation range) is reached. After entering the superelastic region, it is clearly visible that the temperature increases
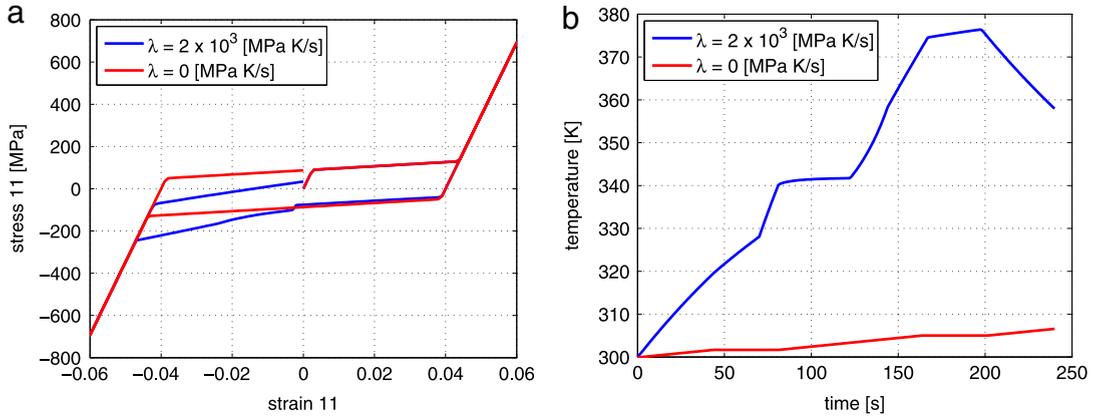
Fig. 5. First strain history: comparison of the strain 11 versus stress 11 plots (a) and of the temperature trends (b) in the two cases heat exchange (blue) versus adiabatic (red). (For interpretation of the references to color in this figure legend, the reader is referred to the web version of this article.)
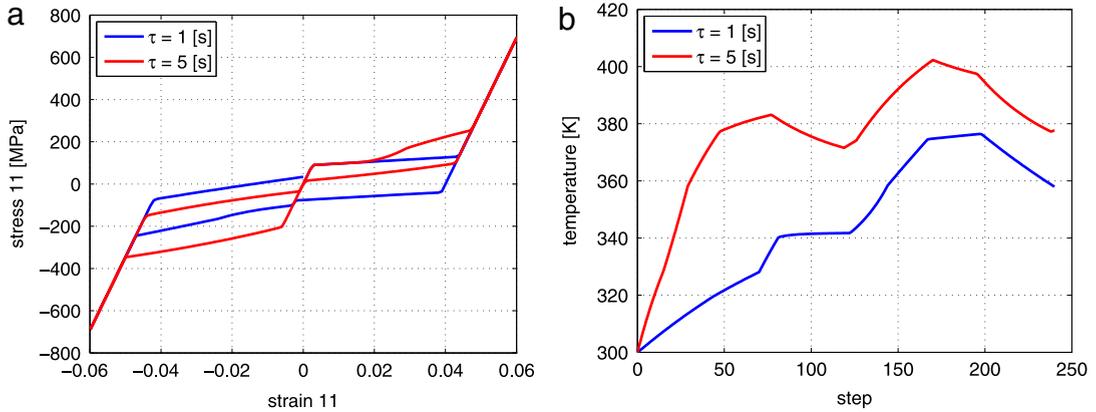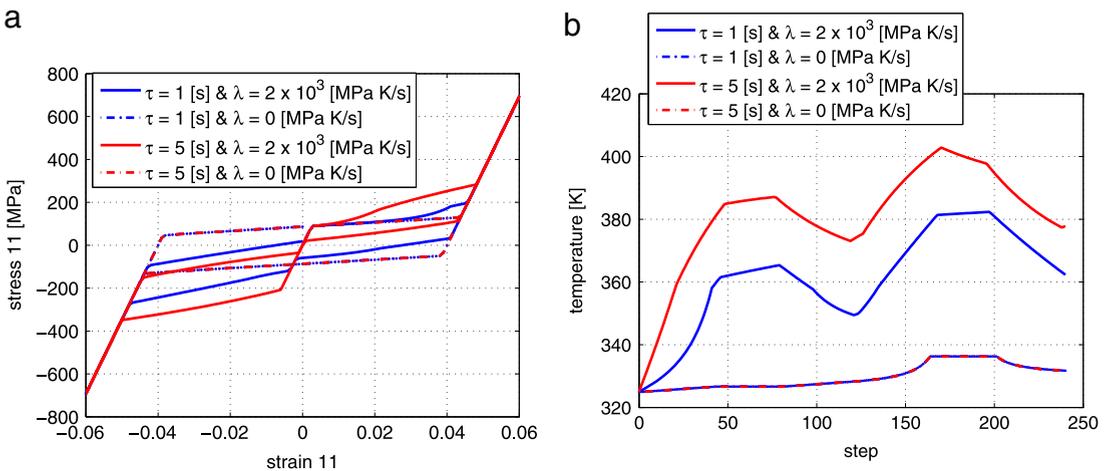

Fig. 6. First strain history: comparison of the strain 11 versus stress 11 plots (a) and of the temperature trends (b) in the two cases $\tau = 1$ s (blue) versus $\tau = 5$ s (red). (For interpretation of the references to color in this figure legend, the reader is referred to the web version of this article.)

Fig. 7. First strain history: comparison of the strain 11 versus stress 11 plots (a) and of the temperature trends (b) for changing rate and heat exchange coefficient. (For interpretation of the references to color in this figure legend, the reader is referred to the web version of this article.)
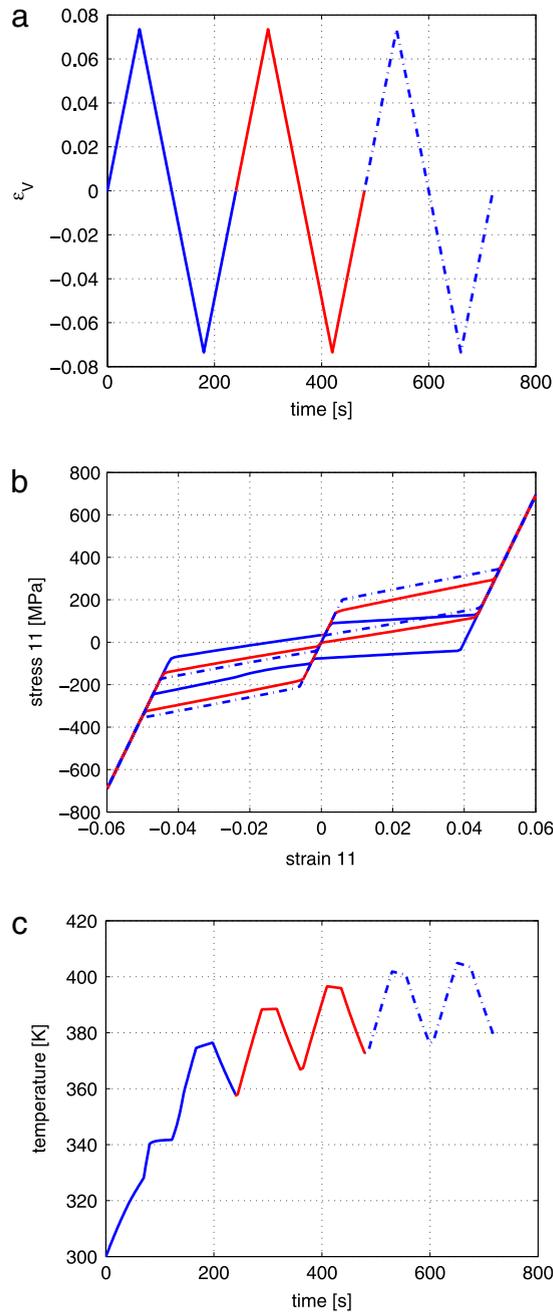
Fig. 8. Second strain history: trend of the variable ε_V (a), strain 11 versus stress 11 plot (b) and temperature trend plot (c). Each traction–compression cycle is highlighted with a different color. (For interpretation of the references to color in this figure legend, the reader is referred to the web version of this article.)

with the increase of the transformation strain during forward phase transformations, and afterwards the temperature decreases (despite the always present environmental heat exchange) during the transformation strain recovery. During the elastic ranges, the temperature changes are only driven by the exchange with the external environment.

In Fig. 5 we compare the above-described response with the case of no heat exchange with the external environment ($\lambda = 0$). In the adiabatic case, the material does not reach the transformation temperature, so there is no temperature decrease due to recovery. The absence of heat exchange is particularly visible during the elastic steps, when the temperature curve in the adiabatic case is flat, while in the former case it relaxes towards the external temperature.
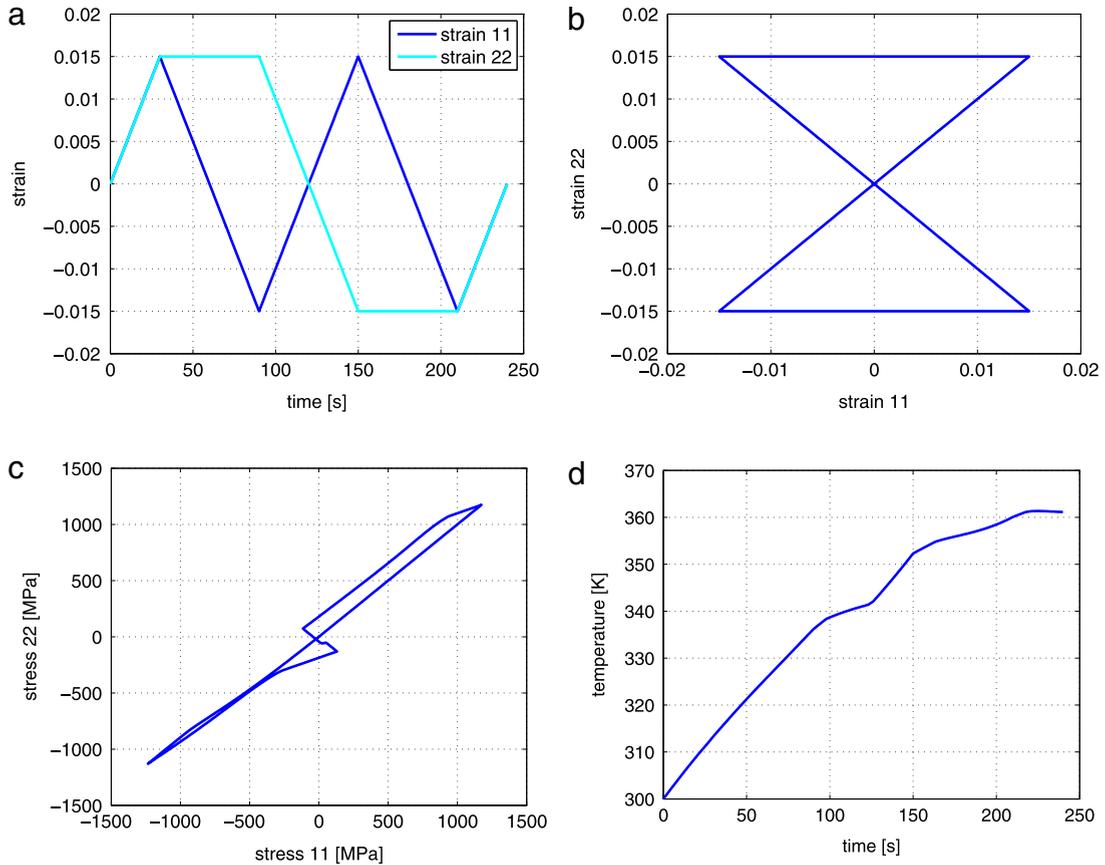
Fig. 9. First hourglass strain history: trend of the strain 11 and strain 22 components (a), strain 11 versus strain 22 plot (b), stress 11 versus stress 22 plot (c) and temperature trend plot (d). (For interpretation of the references to color in this figure legend, the reader is referred to the web version of this article.)

A second comparison is made between the situation of Fig. 4 and a case where the strain–load ε_V is modified in rate as $t \mapsto \varepsilon_V(t/5)$. In Fig. 6 the response of the two cases is compared. The influence of the change in rate is clearly visible. Indeed, the exchange of heat with the environment makes the model rate-dependent. In order to clarify this concept, a further simulation has been performed to compare different loading rates, in both heat exchange and adiabatic cases. An initial temperature equal to 325 K has been chosen in this case. The results of such a comparison are highlighted in Fig. 7, where it is easy to see that in the adiabatic case the variation of the loading rate does not affect the response, i.e., the adiabatic case is rate-independent: indeed, the curves related to the adiabatic situations exactly overlap.

A second choice for $t \mapsto \varepsilon_V(t)$ is a multi-cycle test, displayed in Fig. 8(a). Each cycle is highlighted with a different color, for better readability. The corresponding material response is reported in Fig. 8(b)–(c). Also here, it is apparent that during the forward transformation the temperature increases with the increasing transformation strain, while on the contrary, during the reverse transformation the temperature decreases with the decreasing transformation strain, a behavior proved by several experimental evidences [60,61] and correctly reproduced by the present model.

5.5. Non-proportional tests

We present here also the material response for non-proportional biaxial tests. We perform two hourglass tests as well as a square test. The first hourglass test and the square test present the following strain tensor form

$$
t \mapsto \boldsymbol{\varepsilon}(t) = \begin{bmatrix} \varepsilon_{11}(t) & 0 & 0 \\ 0 & \varepsilon_{22}(t) & 0 \\ 0 & 0 & 0 \end{bmatrix}
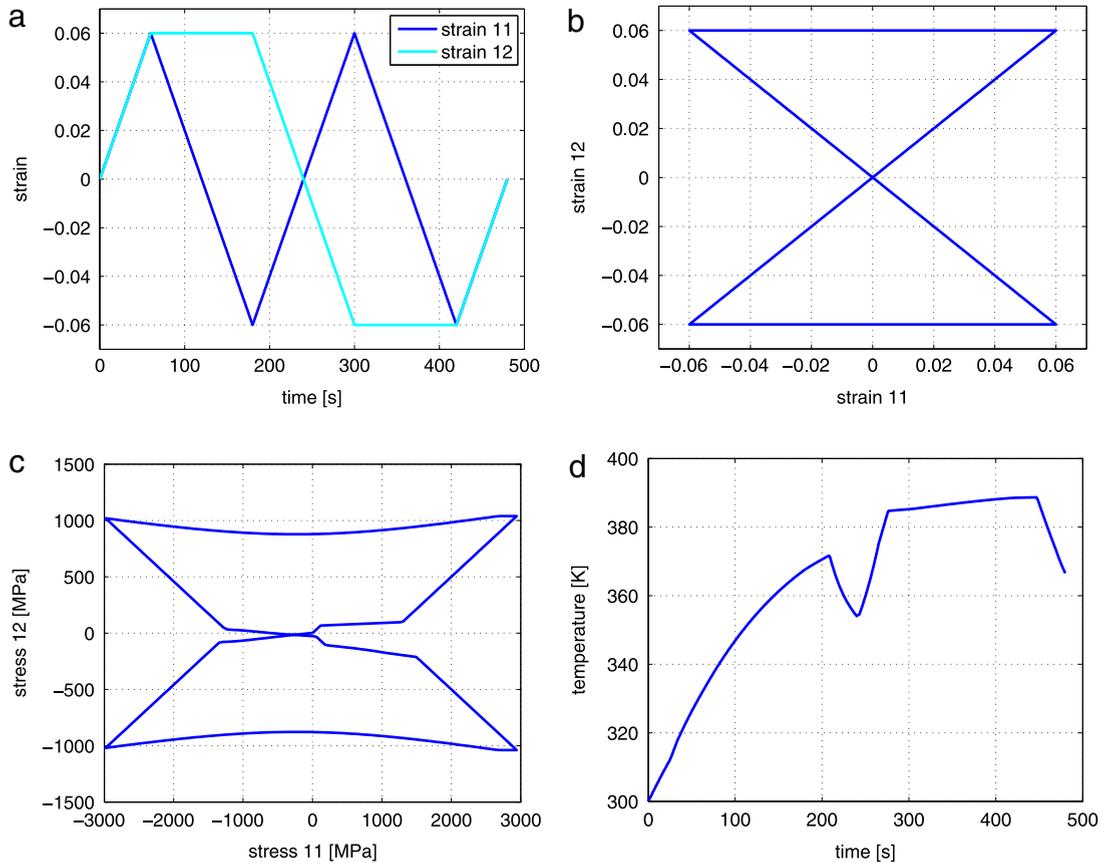$$

Fig. 10. Second hourglass strain history: trend of the strain 11 and strain 12 components (a), strain 11 versus strain 12 plot (b), stress 11 versus stress 12 plot (c) and temperature trend plot (d). (For interpretation of the references to color in this figure legend, the reader is referred to the web version of this article.)

where the two components $t \mapsto \varepsilon_{11}(t)$ and $t \mapsto \varepsilon_{22}(t)$ are given. The strain tensor of the second hourglass test is instead

$$t \mapsto \boldsymbol{\varepsilon}(t) = \begin{bmatrix} \varepsilon_{11}(t) & \varepsilon_{12}(t) & 0 \\ \varepsilon_{12}(t) & 0 & 0 \\ 0 & 0 & 0 \end{bmatrix}$$

with $t \mapsto \varepsilon_{11}(t)$ and $t \mapsto \varepsilon_{12}(t)$ given.

In Figs. 9–11 the imposed strain and the response in terms of stress/strain and temperature plots are presented. The results show that the model is capable of describing the coupled thermomechanical effects also in non-proportional tests.

5.6. Thermal tests

A set of thermal tests are presented, where a constant strain, with the same tensor form of the proportional tests and $\varepsilon_V = 0.044$, is imposed and the external temperature is cycled between 300 and 500 K. Such test setting aims at reproducing material activation in a constraining environment. Different heating/cooling rates have been imposed in order to compare the time-dependent results. The curves are displayed in Fig. 12: the model can properly reproduce a shape-memory actuator response. It can be noted from the results reported in Fig. 12 that as the heating/cooling rate gets lower (i.e. the time step τ gets higher) the material temperature curve gets more and more similar to the external temperature curve, because the heat exchanged with the environment during each time step increases. Accordingly, the difference between maximum and minimum stress is higher, resulting in an enhanced actuation. It can be highlighted
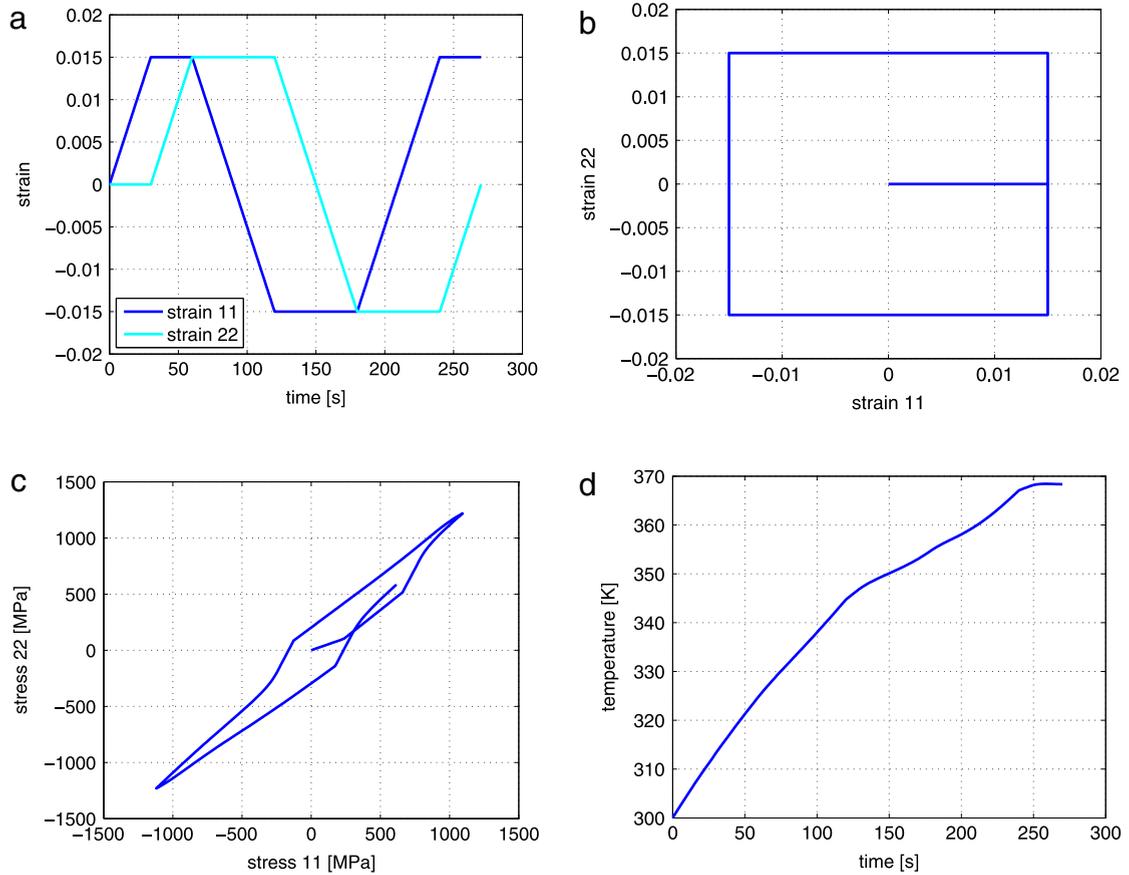
Fig. 11. Square strain history: trend of the strain 11 and strain 22 components (a), strain 11 versus strain 22 plot (b), stress 11 versus stress 22 plot (c) and temperature trend plot (d). (For interpretation of the references to color in this figure legend, the reader is referred to the web version of this article.)
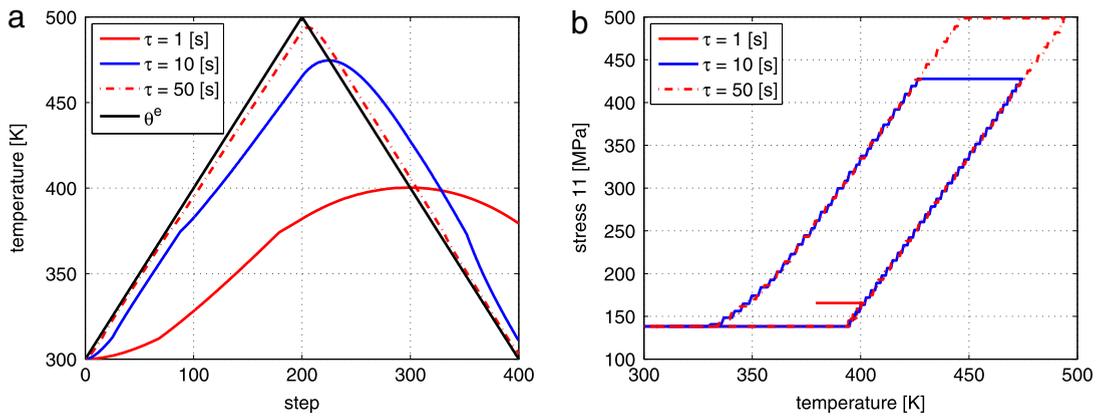

Fig. 12. Thermal tests: comparison of the temperature plots (a) and of the temperature versus stress 11 plots (b) for changing heating/cooling rate. (For interpretation of the references to color in this figure legend, the reader is referred to the web version of this article.)

that for $\tau = 1$ s, i.e. for the highest heating/cooling rate of the three, the actuation cycle is not even completed, since the material temperature does not have enough time to decrease under the transformation temperature.

6. Conclusions

Inspired by the GENERIC variational framework, we have presented a reformulation of a thermomechanically coupled model for SMA in terms of a generalized gradient flow of thermal and mechanical variables. This reformulation has been then specialized to the case of space-homogeneous fields, where it is coordinated with heat exchange with the external environment, here responsible for the rate-dependence in the model.

Based on this reformulation, a semi-implicit time-discrete scheme for the thermomechanically coupled system in the space-homogeneous setting has been presented. The scheme is proved to be unconditionally stable and convergent. In particular, the corresponding continuous counterpart admits a solution.

The performance of the time discretization has been assessed through a number uniaxial and biaxial numerical tests. At the algorithmical level, the nonlinear character of the constitutive model is resolved by a dedicated testing procedure, combined with the solution of a smooth differential system. The computational results prove that the model properly and robustly reproduces the thermomechanical behavior of the material with respect to different loading and environmental regimes.

References

[1] J. Jani, M. Leary, A. Subic, M. Gibson, A review of shape memory alloy research, applications and opportunities, Mater. Des. 56 (2014) 1078–1113.

[2] A.C. Souza, E.N. Mamiya, N. Zouain, Three-dimensional model for solids undergoing stress-induced tranformations, Eur. J. Mech. A Solids 17 (1998) 789–806.

[3] F. Auricchio, L. Petrini, A three-dimensional model describing stress-temperature induced solid phase transformations. Part I: Solution algorithm and boundary value problems, Int. J. Numer. Methods. Eng. 61 (2004) 807–836.

[4] F. Auricchio, L. Petrini, A three-dimensional model describing stress-temperature induced solid phase transformations. Part II: Thermomechanical coupling and hybrid composite applications, Internat. J. Numer. Meth. Engrg. 61 (2004) 716–737.

[5] B. Halphen, Q.S. Nguyen, Sur les matériaux standards généralisés, J. Méchanique 14 (1975) 39–63.

[6] J. Rice, Inelastic constitutive relations for solids: an internal-variable theory and its applications to metal plasticity, J. Mech. Phys. Solids 19 (1971) 203–240.

[7] H. Ziegler, C. Wehrli, The derivation of constitutive relations from the free energy and the dissipation function, in: Advances in Applied Mechanics, vol. 25, Academic Press, Orlando FL, 1987, pp. 183–237.

[8] D. Grandi, U. Stefanelli, The Souza-Auricchio model for shape-memory alloys, Discrete Contin. Dyn. Syst. 8 (4) (2015) 727–743.

[9] F. Auricchio, A. Coda, A. Reali, M. Urbano, SMA numerical modeling versus experimental results: Parameter identification and model prediction capabilities, J. Mater. Eng. Perform. 18 (5–6) (2009) 649–654.

[10] G. Attanasi, F. Auricchio, M. Urbano, Theoretical and experimental investigation on SMA superelastic springs, Journal of Materials Engineering and Performance 20 (4–5) (2011) 706–711.

[11] M. Grmela, H.C. Öttinger, Dynamics and thermodynamics of complex fluids. I. Development of a general formalism, Phys. Rev. E (3) 56 (6) (1997) 6620–6632.

[12] H.C. Öttinger, Beyond Equilibrium Thermodynamics, John Wiley, New Jersey, 2005.

[13] A. Mielke, Formulation of thermoelastic dissipative material behavior using GENERIC, Contin. Mech. Thermodyn. 23 (3) (2011) 233–256.

[14] A. Mielke, Dissipative quantum mechanics using GENERIC, in: Proc. of the Conference on Recent Trends in Dynamical Systems, in: Proceedings in Mathematics & Statistics, vol. 35, Springer, 2013, pp. 555–585.

[15] M.H. Duong, M.A. Peletier, J. Zimmer, GENERIC formalism of a Vlasov–Fokker–Planck equation and connection to large-deviation principles, Nonlinearity 26 (2013) 2951–2971.

[16] A. Mielke, On thermodynamically consistent models and gradient structures for thermoplasticity, GAMM-Mitt. 34 (1) (2011) 51–58.

[17] A. Mielke, A. Petrov, Thermally driven phase transformation in shape-memory alloys, Adv. Math. Sci. Appl. 17 (2007) 667–685.

[18] A. Mielke, L. Paoli, A. Petrov, On existence and approximation for a 3D model of thermally induced phase transformations in shape-memory alloys, SIAM J. Math. Anal. 41 (2009) 1388–1414.

[19] T. Roubíček, U. Stefanelli, Magnetic shape-memory alloys: thermomechanical modeling and analysis, Contin. Mech. Thermodyn. 26 (2014) 783–810.

[20] P. Krejčí, U. Stefanelli, Well-posedness of a thermo-mechanical model for shape memory alloys under tension, M2AN Math. Model. Numer. Anal. 44 (6) (2010) 1239–1253.

[21] P. Krejčí, U. Stefanelli, Existence and nonexistence for the full thermomechanical Souza-Auricchio model of shape memory wires, Math. Mech. Solids 16 (2011) 349–365.

[22] F. Auricchio, E. Bonetti, A new "flexible" 3D macroscopic model for shape memory alloys, Discrete Contin. Dyn. Syst. Ser. S 6 (2) (2013) 277–291.

[23] F. Auricchio, J. Lubliner, A uniaxial model for shape-memory alloys, In. J. Solids Struct. 34 (1997) 3601–3618.

[24] S. Govindjee, C. Miehe, A multi-variant martensitic phase transformation model: Formulatin and numerical implementation, Comput. Methods Appl. Mech. Engrg. 191 (2001) 215–238.

[25] D. Helm, P. Haupt, Shape memory behaviour: modelling within continuum thermomechanics, Int. J. Solids Struct. 40 (2003) 827–849.

[26] V.I. Levitas, Thermomechanical theory of martensitic phase transformations in inelastic materials, Intern. J. Solids Struct. 35 (1998) 889–940.

[27] B. Peultier, T. Ben Zineb, E. Patoor, Macroscopic constitutive law for SMA: Application to structure analysis by FEM, Mater. Sci. Eng. A 438–440 (2006) 454–458.

[28] P. Popov, D.C. Lagoudas, A 3-D constitutive model for shape memory alloys incorporating pseudoelasticity and detwinning of self-accommodated martensite, Int. J. Plast. 23 (2007) 1679–1720.

[29] B. Raniecki, Ch. Lexcellent, R_L models of pseudoelasticity and their specification for some shape-memory solids, Eur. J. Mech. A Solids 13 (1994) 21–50.

[30] S. Reese, D. Christ, Finite deformation pseudo-elasticity of shape memory alloys — constitutive modelling and finite element implementation, Int. J. Plasticity 24 (2008) 455–482.

[31] P. Thamburaja, L. Anand, Polycrystalline shape-memory materials: effect of crystallographic texture, J. Mech. Phys. Solids 49 (2001) 709–737.

[32] D.C. Lagoudas, P.B. Entchev, P. Popov, E. Patoor, L.C. Brinson, X. Gao, Shape memory alloys, Part II: Modeling of polycrystals, Mech. Mater. 38 (2006) 391–429.

[33] D. Lagoudas, S. Hartl, Y. Cheminsky, L. Machado, P. Popov, Constitutive model for the numerical analysis of phase transformation in polycrystalline shape memory alloys, Int. J. Plasticity 32–33 (2012) 155–183.

[34] R. Mirzaeifar, R. DesRoches, A. Yavari, Analysis of the rate-dependent coupled thermo-mechanical response of shape memory aloys bars and wires in tension, Contin. Mech. Thermodyn. 23 (2011) 363–385.

[35] R. Mirzaeifar, R. DesRoches, A. Yavari, K. Gall, Coupled thermo-mechanical analysis of shape memory alloy circular bars in pure tension, Int. J. Nonlinear. Mech. 47 (2012) 118–128.

[36] C. Morin, Z. Moumni, W. Zaki, A constitutive model for shape memory accounting for thermomechanical coupling, Int. J. Plasticity 27 (2011) 748–767.

[37] F. Auricchio, A. Reali, U. Stefanelli, A macroscopic 1D model for shape memory alloys including asymmetric behaviors and transformation-dependent elastic properties, Comput. Methods Appl. Mech. Eng. 198 (2009) 1631–1637.

[38] F. Auricchio, A.-L. Bessoud, A. Reali, U. Stefanelli, A phenomenological model for the magneto-mechanical response of single-crystal magnetic shape memory alloys, Eur. J. Mech. A Solids 52 (2015) 1–11.

[39] A.-L. Bessoud, M. Kružík, U. Stefanelli, A macroscopic model for magnetic shape memory alloys, Z. Angew. Math. Phys. 64 (2) (2013) 343–359.

[40] A.-L. Bessoud, U. Stefanelli, Magnetic shape memory alloys: Three-dimensional modeling and analysis, Math. Models Methods Appl. Sci. 21 (2011) 1043–1069.

[41] U. Stefanelli, Magnetic control of magnetic shape-memory single crystals, Physica B 407 (2012) 1316–1321.

[42] F. Auricchio, A. Reali, U. Stefanelli, A three-dimensional model describing stress-induces solid phase transformation with residual plasticity, Int. J. Plasticity 23 (2007) 207–226.

[43] M. Eleuteri, L. Lussardi, U. Stefanelli, A rate-independent model for permanent inelastic effects in shape memory materials, Netw. Heterog. Media 6 (2011) 145–165.

[44] V. Evangelista, S. Marfia, E. Sacco, Phenomenological 3D and 1D consistent models for shape-memory alloy materials, Comput. Mech. 44 (2009) 405–421.

[45] S. Frigeri, U. Stefanelli, Existence and time-discretization for the finite-strain Souza-Auricchio constitutive model for shape-memory alloys, Contin. Mech. Thermodyn. 24 (2012) 63–77.

[46] A. Mielke, L. Paoli, A. Petrov, U. Stefanelli, Error estimates for space–time discretizations of a rate-independent variational inequality, SIAM J. Numer. Anal. 48 (2010) 1625–1646.

[47] M. Peigney, A time-integration scheme for thermomechanical evolutions of shape-memory alloys, C. R. Mec. 334 (2006) 266–271.

[48] M. Peigney, J.P. Seguin, An incremental variational approach to coupled thermo-mechanical problems in anelastic solids. Application to shape-memory alloys, Int. J. Solids Struc. 50 (2013) 4043–4054.

[49] F. Auricchio, L. Petrini, Improvements and algorithmical considerations on a recent three-dimensional model describing stress-induced solid phase transformations, Internat. J. Numer. Methods Engrg. 55 (2002) 1255–1284.

[50] F. Auricchio, A. Mielke, U. Stefanelli, A rate-independent model for the isothermal quasi-static evolution of shape-memory materials, Math. Models Methods Appl. Sci. 18 (2008) 125–164.

[51] V. Evangelista, S. Marfia, E. Sacco, A 3D SMA constitutive model in the framework of finite strain, Internat. J. Numer. Methods Engrg. 81 (2010) 761–785.

[52] F. Auricchio, A. Reali, U. Stefanelli, A phenomenological 3D model describing stress-induced solid phase transformations with permanent inelasticity, in: B. Miara, G. Stavroulakis, V. Valente (Eds.), Topics on Mathematics for Smart Systems, World Sci. Publ., Hackensack, NJ, 2007, pp. 1–14.

[53] D. Grandi, U. Stefanelli, A phenomenological model for microstructure-dependent inelasticity in shape-memory alloys, Meccanica 49 (9) (2014) 2265–2283.

[54] F. Auricchio, A.-L. Bessoud, A. Reali, U. Stefanelli, A three-dimensional phenomenological models for magnetic shape memory alloys, GAMM-Mitt. 34 (2011) 90–96.

[55] A. Mielke, L. Paoli, A. Petrov, U. Stefanelli, Error bounds for space–time discretizations of a 3d model for shape-memory materials, in: K. Hackl (Ed.), IUTAM Symposium on Variational Concepts with Applications to the Mechanics of Materials, Springer, 2010, pp. 185–197. Proceedings of the IUTAM Symposium on Variational Concepts, Bochum, Germany, Sept. 22–26, 2008.

[56] M. Eleuteri, L. Lussardi, Thermal control of a rate-independent model for permanent inelastic effects in shape memory materials, Evol. Equ. Control Theory 3 (2014) 411–427.

[57] M. Eleuteri, L. Lussardi, U. Stefanelli, Thermal control of the souza-auricchio model for shape memory alloys, Discrete Cont. Dyn. Syst. Ser. S 6 (2013) 369–386.

[58] H. Brézis, Operateurs maximaux monotones et semi-groupes de contractions dans les espaces de Hilbert, in: Math Studies, vol. 5, North-Holland, Amsterdam, New York, 1973.

[59] F. Auricchio, G. Scalet, M. Urbano, A numerical/experimental study of nitinol actuator springs, J. Mater. Engrg. Perform. 23 (2014) 2420–2428.

[60] R. Peyroux, A. Chrysochoos, Ch. Licht, M. Löbel, Thermomechanical couplings and pseudoelasticity of shape memory alloys, Internat. J. Engrg. Sci. 36 (1998) 489–509.

[61] R. Peyroux, A. Chrysochoos, Ch. Licht, M. Löbel, Phenomenological constitutive equations for numerical simulations of SMA's structures. Effect of thermomechanical couplings, J. Phys. C4 Suppl. 6 (1996) 347–356.